Geografia Fisica e Dinamica Quaternaria
GFDQ 47 (2024), 329-348

DOI 10.4454/gtr56snb

Silvia BERTOLI[1], Maria Cristina SALVATORE[2*], Andrea PACIFICI[3], Carlo BARONI[2]

Geomorphological and Photogeological Units Map of Cilaos Crater: interpretation of landforms and surface processes in Eastern Promethei Terra, Mars

Abstract: Bertoli S., Salvatore M.C., Pacifici A., Baroni C., *Geomorphological and Photogeological Units Map of Cilaos Crater: interpretation of landforms and surface processes in Eastern Promethei Terra, Mars.* (IT ISSN 0391-9838, 2024). A detailed geomorphological mapping is essential to describe the spatial distribution, morphometry, and genesis of Martian landforms, and to better understand the processes that have shaped and continue to influence the planet's surface morphology. However, high-resolution thematic cartography of Mars is still largely lacking despite its critical importance for the interpretation of surface processes and the planning of future exploration missions. This study focuses on Cilaos Crater (35.72° S, 129.45° E, eastern Promethei Terra), a site of particular interest due to the presence of the young Gasa Crater (7 km in diameter) within its boundaries. We present a detailed geomorphological map of the Cilaos region, created through remote sensing analysis using high-resolution imagery from the Mars Reconnaissance Orbiter and topographic data from the Mars Orbiter Laser Altimeter (MOLA), processed within a GIS framework. Photointerpretation allowed us to produce a 1:25,000 scale geomorphological map, differentiating photogeological units as well as erosional and depositional landforms shaped by various morphogenetic processes. Our analysis highlights the significant impact of Gasa Crater's formation on the surrounding landscape. The interaction between the degrading latitude-dependent mantle (LDM) and Gasa's impact ejecta has played a crucial role in shaping flow-like structures and modifying pre existing terrain. This underscores the importance of the interplay of impact events and periglacial environment in shaping the Martian surface during the late Amazonian. Furthermore, by reconstructing the relative chronology of landforms, deposits, and photogeological units, we link the relatively young age of Gasa Crater to the broader landscape evolution of the Cilaos region. This study provides new insights into the ongoing geomorphic processes that continue to shape Mars' mid-latitudes.

Key words: Landscape analysis, Geomorphological mapping, Planetary geomorphology, Remote sensing, Mars.

Riassunto: Bertoli S., Salvatore M.C., Pacifici A., Baroni C., *Carta Geomorfologica e delle Unità Fotogeologiche del Cratere Cilaos: interpretazione delle forme del rilievo e dei processi superficiali nella Promethei Terra orientale, Marte.* (IT ISSN 0391-9838, 2024). La cartografia geomorfologica di dettaglio è fondamentale per descrivere la distribuzione spaziale, la morfometria e la genesi delle forme del rilievo marziane, e per meglio definire i processi che hanno modellato e modellano tuttora la superficie del Pianeta rosso. Tuttavia, la cartografia tematica ad alta risoluzione di Marte risulta ancora largamente carente, nonostante la sua importanza cruciale per l'interpretazione dei processi superficiali e per la pianificazione delle future missioni di esplorazione. Questo studio si concentra sul Cratere Cilaos (35.72° S, 129.45° E, Promethei Terra orientale), un sito di particolare interesse per la presenza al suo interno del giovane Cratere Gasa (7 km di diametro). In questo lavoro presentiamo i risultati dell'analisi delle forme del rilievo della regione di Cilaos, realizzata attraverso l'analisi da remoto mediante immagini ad alta risoluzione del Mars Reconnaissance Orbiter e dati topografici del Mars Orbiter Laser Altimeter (MOLA). L'analisi fotogeologica ha permesso di produrre una carta geomorfologica in scala 1:25,000, nella quale sono distinte unità fotogeologiche e forme del rilievo riconducibili a diversi agenti morfogenetici. La nostra analisi evidenzia l'impatto significativo della formazione del Cratere Gasa sul paesaggio circostante. L'interazione tra il latitude-dependent mantle (LDM) e i prodotti dall'impatto che ha generato il cratere Gasa ha svolto un ruolo cruciale nella formazione di strutture simili a flussi e nella modifica del terreno preesistente, sottolineando l'importanza dell'interazione tra gli eventi di impatto e ambiente periglaciale nel modellamento della superficie di Marte durante il tardo Amazzoniano. Questo studio fornisce nuove informazioni sui processi geomorfologici ancora attivi che continuano a modellare le medie latitudini di Marte.

Termini chiave: Analisi delle forme del rilievo, Cartografia geomorfologica, Geomorfologia planetaria, Telerilevamento, Marte.

INTRODUCTION

A comprehensive understanding of Mars' landscape and climatic evolution requires detailed investigation of surficial landforms. The Martian surface preserves a complex stratigraphic and geomorphological record

[1] *INAF, Osservatorio Astronomico di Padova, Padova, Italy.*
[2] *Department of Earth Sciences, University of Pisa, Pisa, Italy.*
[3] *International Research School of Planetary Sciences, Università d'Annunzio, Pescara, Italy.*
[*] *Corresponding author: Maria Cristina Salvatore (mariacristina.salvatore@unipi.it)*

shaped by multiple surface and impact-related processes, which document the planet's environmental and climatic evolution over time. However, despite decades of planetary exploration, geomorphological mapping on Mars remains limited in scope and resolution compared to terrestrial standards. Most existing maps are produced at small scales, limiting their capacity to capture local variability and morphological transitions, elements crucial for interpreting surface-forming processes. A particularly significant gap in planetary cartography concerns the characterization of mid- to high-latitude terrains, which are extensively mantled by ice-rich deposits. One of the most widespread units in these regions is the Latitude Dependent Mantle (LDM), a metre-thick layer composed of dust, sand, and rock particles cemented by water ice, covering more than 23% of the Martian surface (Kreslavsky and Head, 2002). This unit likely formed through atmospheric deposition during periods of high orbital obliquity (Laskar *et al.*, 2004) acting both as a proxy for recent climate cycles and a potential near-surface water reservoir. Nonetheless, its internal structure, spatial distribution, and interaction with other geological processes – especially impact cratering – remain only partially understood.

This study addresses these gaps through a detailed landscape analysis of the Cilaos-Gasa crater system, located in Promethei Terra (MC-29 Eridania quadrangle), east of the Hellas Basin (fig. 1), which furnished a geomorphological and photogelogical units map at a scale of 1:50,000 (Supplementary Material). The older and larger Cilaos Crater, dated to 572 ± 110 Ma (Lagain *et al.*, 2022) is partly filled by LDM deposits and hosts the younger Gasa Crater (35.72° S, 129.45° E) within its floor. This latter is a 7 km-wide impact structure with a well-preserved rim, ejecta blanket, and relatively flat floor. Considering the state of preservation of Gasa's rays (Schon *et al.*, 2009) the crater's age is estimated to range between 0.6 and 2.4 Ma. Moreover, the ejecta deposits surrounding the Gasa Crater boundary are particularly relevant for constraining its impact age, as their smooth surface allows for reliable crater counting. Based on Hartmann's isochrones (2005), an estimated age of 1.25 Ma has been proposed for Gasa Crater (Malin *et al.*, 2007). The superposition of Gasa within Cilaos, combined with the presence of LDM, creates a unique setting where impact-related processes and climate-driven deposits directly interact. The high-resolution geomorphological mapping of the Cilaos–Gasa system presented in this study aims to characterize the landscape evolution of a mid-latitude Martian landscape shaped by the interplay of impact cratering, ice-rich mantling, and possible periglacial activity.

Particular attention is given to the spatial and genetic relationships between Gasa's ejecta and the underlying LDM, which provide new insights into resurfacing dynamics and obliquity-driven ice redistribution. Beyond refining the understanding of surface evolution in Promethei Terra, these results inform broader reconstructions of recent environmental variability across Mars. Crucially, the identification and mapping of features indicative of ground ice stability and degradation contribute to the detection of near-surface volatile reservoirs. This information is essential for constraining the environmental significance of recent landscape evolution and for driving the selection of future landing sites in regions with high astrobiological and in-situ resource potential.

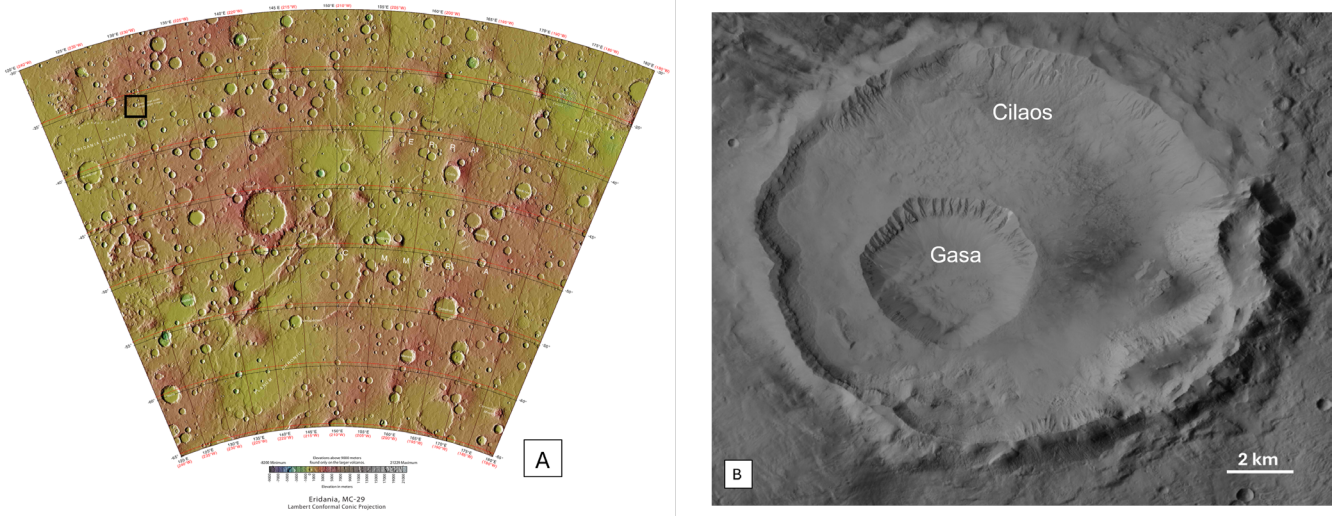

Figure 1 - A) Eridania quadrangle topographic map (http://planetarynames.wr.usgs.gov/images/mc29_mola.pdf). The black rectangle indicates the study area. B) Hillshade image of the Cilaos and Gasa craters derived from CTX image (P08_004060_1440_XI_36S230W) (35.72° S, 129.45° E).

MATERIAL AND METHODS

The geomorphological map of the Cilaos Crater was compiled through the interpretation of remote sensing data. Access to datasets from the Mars Orbital Data Explorer of the Planetary Data System Geoscience Node (NASA) and available catalogs from the Lunar and Planetary Laboratory (LPL) enabled the integration of both high-resolution imagery and digital terrain models (DTMs).

Photointerpretation was performed using selected data from the Mars Reconnaissance Orbiter (MRO). Specifically, a 6 m/px spatial resolution image from the CTX (Context Camera, Malin *et al.*, 2007) provided a general overview of the study area, while eight HiRISE (High-Resolution Imaging Science Experiment, McEwen *et al.*, 2007) images with a spatial resolution of 0.25 m were used for detailed analyses.

To enhance the landscape and morphometric analysis, two high-resolution DTMs (1 m/px nominal resolution) derived from HiRISE stereo pairs were utilized. Additionally, a third DTM was generated from another set of HiRISE stereo pairs (e.g., PSP_005616_1440 and ESP_011536_1440) using the NASA Ames Stereo Pipeline (Beyer *et al.*, 2018). The processing included photogrammetric bundle adjustment, sub-pixel stereo correlation, and terrain model construction through stereo photogrammetry. The final DTM was aligned to the MOLA global topographic reference frame in ASP, ensuring consistency in absolute elevation values. The nominal horizontal resolution of the DTM is ~1 m/pixel, with an estimated vertical precision of ~0.25-1 m depending on terrain slope and image quality. This level of precision is adequate for the morphometric and topographic analyses conducted in this work, such as slope profiling and relative elevation measurements across geomorphic features. This additional DTM was necessary to address gaps in coverage, particularly along the eastern inner margin of Cilaos.

Data from the High-Resolution Stereo Camera (HRSC, (Neukum and Jaumann, 2004; Jaumann *et al.*, 2007) aboard the Mars Express orbiter were also incorporated. The HRSC system, a multi-sensor push-broom instrument, provided a digital terrain model from stereo image pairs with a spatial resolution of 75 m. This dataset was used to orthorectify the CTX image and extract contour lines overlapping the orthophotos.

The images were imported into a Geographic Information System (QGIS) and georeferenced using the georeferencing tool. CTX imagery was used as the base reference layer. HiRISE images were manually georeferenced in QGIS using the georeferencing tool, with surface features aligned to the CTX base map. All layers were projected in the Mars Equidistant Cylindrical projection (central meridian 0° E), consistent with the MOLA reference system. HiRISE DTMs were used primarily for local-scale spatial visualization of individual events and morphologic units. Depth measurements for Cilaos and Gasa craters were derived from HRSC DTMs, which offer reliable vertical accuracy for regional-scale topographic analysis. The list of the images used with information on ID number, mission, camera instrument, and key geometric parameters is reported in Table S1 (Supplementary Material). Landforms and photogeological units were identified through photointerpretation, considering variations in tone, texture, structure, size, and shape. The collected data were manually digitized and stored in vector format (*.shp) as points, lines, or polygons, depending on their geometry, using the open-source GIS software Quantum GIS (QGIS 3.22.11). Mapping was performed at a scale of 1:2000, which we consider appropriate considering the spatial resolution of the base data (0.25 m/pixel) and the objectives of the study. This scale allows for the identification and classification of key morphologies while minimizing overinterpretation of features below the data's effective resolution.

The legend adopted for the geomorphological map follows the terrestrial geomorphological classification, with modifications where necessary, according to (Campobasso *et al.*, 2018). Photogeological units were categorized into two main groups based on their relationship with the Cilaos and Gasa craters. Landforms were differentiated by color according to their morphogenetic processes, while specific symbols indicated structural features and geometric characteristics. Features of uncertain origin were depicted in black to reflect this ambiguity, thereby avoiding premature classification.

Although geomorphological maps of the Earth typically distinguish between active and inactive landforms, with active landforms being those found in the morphoclimatic conditions where they were formed, this distinction was not applied in the present study. In fact, the context of Martian geomorphology, it is often challenging to definitively assign a feature to a particular state of activity due to the complex and sometimes ambiguous nature of the processes involved, which are often slow, intermittent, or seasonal, making it difficult to distinguish between inactive and active landforms.

LANDFORMS AND DEPOSITS OF CILAOS AND GASA CRATERS

Impact landforms

The study area is characterized by two prominent impact landforms: Cilaos and Gasa. Cilaos Crater is the largest, covering approximately 1340 km², reaching an average depth of 1.28 km, and hosting the smaller Gasa Crater. The latter extends over ~49 km² and reaches a maximum depth of 0.8 km.

Numerous smaller craters are scattered within Cilaos Crater, exhibiting diameters ranging from 27 m to 418 m.

These craters are filled with fine-grained sediments displaying parallel linear structures associated with aeolian processes (longitudinal dunes). Primarily located along the southern inner wall of Cilaos Crater, these small impact features define the "Densely Cratered Inner Wall Unit" (fig. 2; see photogeological units paragraph). The small craters identified in the Cilaos region are mostly like resulting from the ballistic emplacement of ejecta produced during the Gasa impact event.

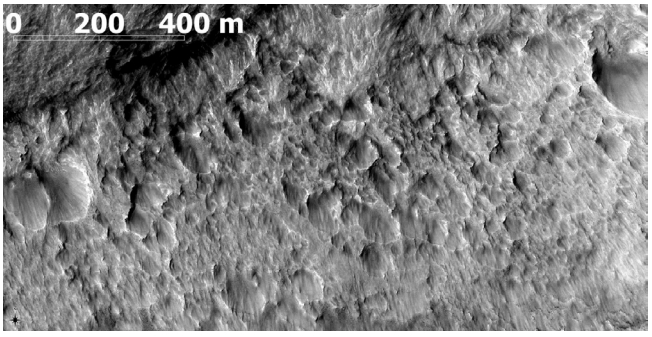

Figure 2 - Small impact craters on Cilaos Crater.

Aeolian landforms and deposits

Parallel linear structures are widespread throughout the study area and are interpreted as Transversal Aeolian Ridges (TARs, fig. 3). Predominantly found in the eastern sector of Cilaos Crater, TARs range in length from a few meters to ~50 m, with widths below 2 m, and are generally oriented SW-NE. Neighboring dunes often merge, forming sinuous and complex patterns. Although the available DTM does not allow for 3D visualization of individual dunes, the contrast between illuminated and shaded areas in HiRISE images was used to infer windward and leeward slopes, suggesting a prevailing wind direction from NW to SE.

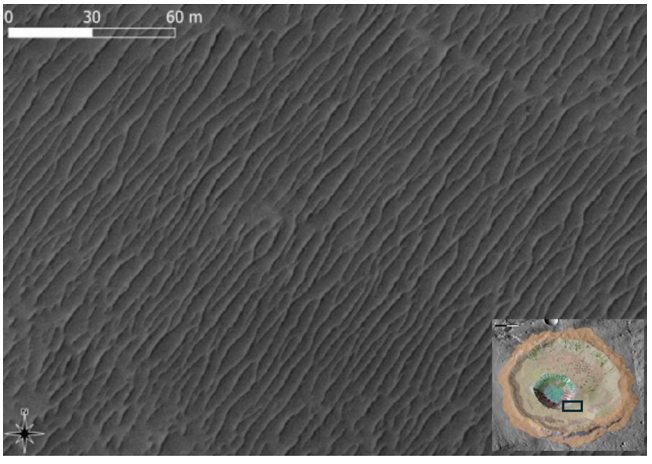

Figure 3 - Transversal Aeolian Ridges (TARS) on the floor of the Cilaos Crater. Their morphology and alignment are indicative of prevailing wind directions at the time of formation (HiRISE ESP_021584_1440).

Geometric patterns cover the floor of Gasa Crater (fig. 4). The cells range in size from ~5 m to over 100 m, exhibiting irregular and sharp-edged patterns. These features are interpreted as star dune fields, with fine-grained material at the dune bases following a similar configuration. Dune size decreases towards the southern portion of the crater.

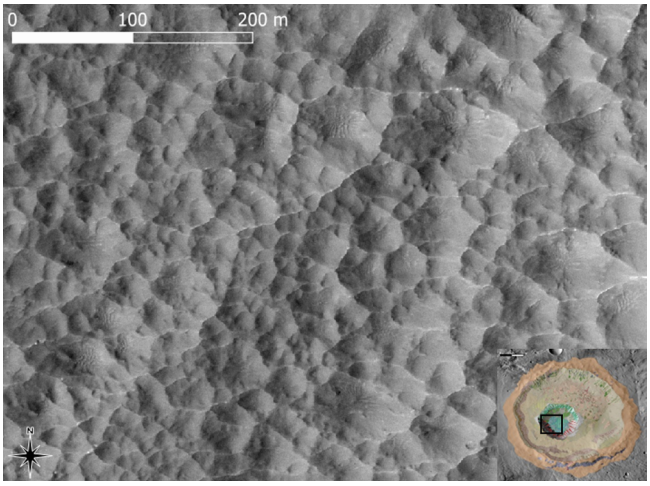

Figure 4 - Star dunes on the Gasa floor (HiRISE ESP_021584_1440).

A transition from transverse dunes to star dunes is observed in the southeastern sector of Gasa Crater. Near its rim, star dunes exhibit rounded edges and appear less well-preserved compared to other areas.

Gravity induced landforms and deposits

Numerous linear features develop along the south-facing slopes of the main impact structures (fig. 5). These features are interpreted as trenches and fractures caused by collapse processes affecting the inner crater walls.

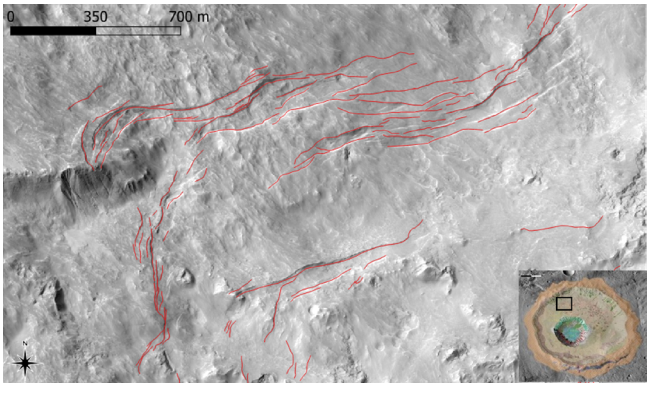

Figure 5 - Collapse structures (in red) observed on the southwestern sector of the Cilaos crater's inner wall (HiRISE ESP_014147_1440_RED).

Rockfall deposits, consisting of plurimetric boulders, are predominantly located on the steepest slopes of the western sector of Cilaos Crater. In several cases, rockfall tracks are preserved along the slopes, indicating rolling motion of the detached blocks (fig. 6).

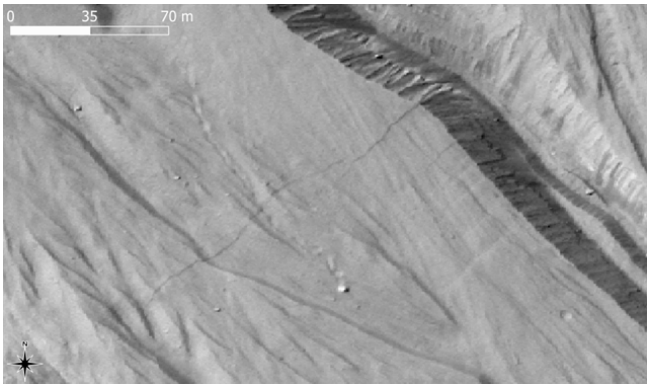

Figure 6 - Rockfall track and deposits on Gasa Crater. Boulder dimension is about 5.5 m length (HiRISE ESP_014147_1440).

The rockfall detachment zones are mainly concentrated in the upper portions of the slopes, primarily along the north-facing walls where the Cilaos and Gasa Bedrock Units outcrop.

A large landslide deposit was identified along the inner wall edge of Cilaos Crater. Based on the observed flow-line structures, this feature has been classified as a mud-flow-like landform.

Two deep-seated gravitational slope deformations (DSGSDs) were recognized along the southeastern inner rim of Cilaos Crater (fig. 7).

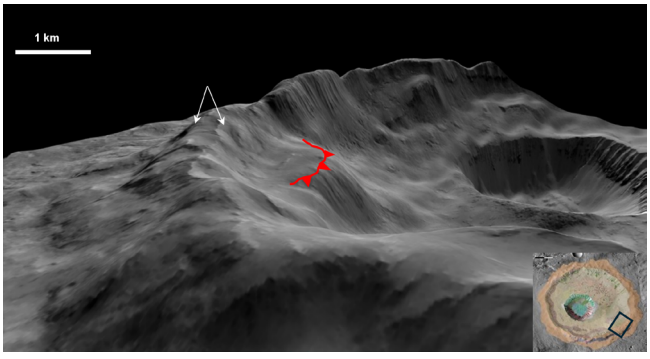

Figure 7 - 3D view of Deep-Seated Gravitational Slope Deformations (DGSDs) with 3× vertical exaggeration. White arrows indicate the presence of a double rim structure along the Cilaos Crater wall. The red line with triangular markers delineates the boundary of the associated terrace.

On Mars DSGSDs are known in many areas and involve low, complex, gravity-driven deformations affecting entire slopes (Peulvast *et al.*, 2001; Kromuszczyńska *et al.*, 2019; Discenza *et al.*, 2021 and reference therein). On Earth, these phenomena typically exhibit deformation rates in the range of millimeters per year (Della Seta *et al.*, 2017), which are negligible when compared to their extensive dimensions (Dramis and Sorriso-Valvo, 1994). DSGSDs in Cilaos Crater are characterized by multiple geomorphic features distributed along the entire ridge-slope-valley system, including double ridges, ridge-top depressions, trenches, and scarps DSGSDs.

Periglacial-like landforms

Polygonal patterns, morphologically comparable to terrestrial periglacial polygons, represent one of the most pervasive surface features observed within the study area. Their widespread distribution suggests the influence of ground ice-related processes, potentially linked to thermal contraction cracking or freeze-thaw cycles, analogous to those occurring in cold-climate environments on Earth.

The first type of polygonal structure is located along the south-facing inner wall of Cilaos Crater, in alcoves or heads of several gullies. These polygons, referred to as "gullygons" or gully polygon systems (sensu Levy *et al.*, 2009, fig. 8), exhibit characteristics of both polygonal networks and gullies, often forming along polygon edges or within degraded polygonal terrains. Their morphology suggests a possible genetic link between periglacial processes (e.g., thermal contraction cracking) and localized mass wasting or liquid-driven erosion. In Cilaos Crater, gullygons show an average diameter of 15 m (measured along the major axis) and exhibit variable shapes, ranging from square to trapezoidal. Their flat surface presents a pseudo-imbricated arrangement resembling fish scales. Their occurrence is relevant as may reflect episodic melting of near-surface ground ice. Levy *et al.* (2008) interpreted gullygons as analogous to composite wedge polygons found in the inland mixed zone of the Antarctic Dry Valleys.

The second type of polygonal structures is found both on the inner wall of Cilaos Crater and on the mudflow deposits within the crater floor. These polygons have an average diameter of about 30 m, develop on sub-flat surfaces, and lack swellings or concavities (fig. 9).

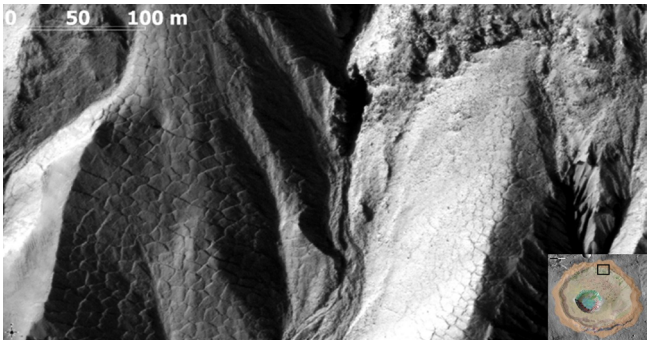

Figure 8 - The fish scales-like disposition of the polygon along the slope (HiRISE ESP_011536_1440_RED).

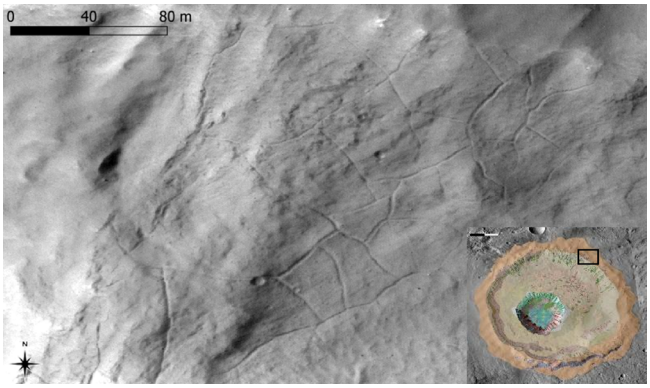

Figure 9 - Polygonal patterned ground in the northeastern part of the Cilaos outer wall (HiRISE ESP_011536_1440_RED).

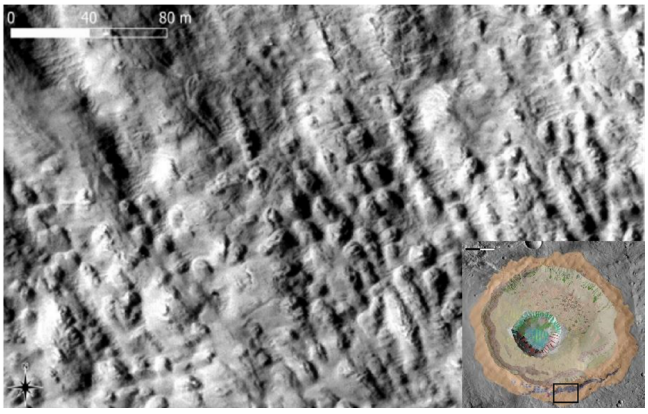

Figure 10 - The pingo like features characterized by a dome shape with a depressed area on top.

Groups of small convex dome-shaped structures, distributed along a linear pattern (fig. 10), are also present in the central part of the outer margin of Cilaos Crater. These features are characterized by small radial fractures at their summits. The domes, which have an average diameter of about 15 m, are interpreted as analogues of terrestrial pingos. The alignment of the pingos along preferred orientations can be attributed to structural control exerted by the underlying bedrock geology, such as fracture networks and/or lithological anisotropies.

Fluvial-like landforms and deposits

Fluvial-like landforms and deposits are widespread throughout the study area, particularly in the inner sectors of Cilaos and Gasa Craters (fig. 11).

Both crater walls exhibit gullies, which are among the most prominent and widely discussed landforms on Mars, often considered key indicators of past aqueous activity and erosional processes. Martian gullies are composite features, typically consisting of an alcove, a channel, and a depositional fan (apron) (Malin and Edgett, 2000). Their lengths range from a few meters to several kilometers, and they usually occur in groups. Gullies are predominantly found at mid-latitudes (with only a few in polar regions) and form on moderate to steep slopes (Reiss *et al.*, 2009; Conway *et al.*, 2015, 2019), affecting central crater peaks, walls, valley slopes, and hills (Malin and Edgett, 2000; Balme *et al.*, 2006).

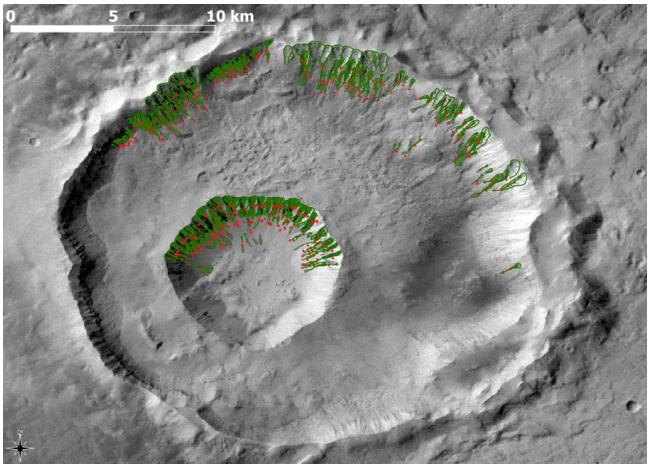

Figure 11 - Panoramic view of the gullies within Cilaos and Gasa craters (CTX P08_004060_1440_XI_36S230W).

Several models attempt to explain their formation, including dry granular flows (Treiman, 2003)), fluvial flow mechanisms (Conway *et al.*, 2015; Hobbs *et al.*, 2017; Yue *et al.*, 2014), and debris flows (Miyamoto *et al.*, 2004; Mangold *et al.*, 2010; Jouannic *et al.*, 2019). Terrestrial analogues have played and continue to play a crucial role in supporting different hypotheses. It is now widely accepted that gullies are formed by a fluid, whether liquid water (H_2O) or gaseous CO_2 (Diniega *et al.*, 2010; Dundas *et al.*, 2010, 2017; Raack *et al.*, 2015; Pasquon *et al.*, 2016). Here, we classify Martian gullies as fluvial-like landforms, drawing parallels to terrestrial debris flows based on their morphological similarities and inferred processes. In our study area, gullies are located on the south-facing inner walls of both craters. These features display well-developed alcoves, which are erosional basins formed due to headward retreat. Based on the degree of erosion, which can be evaluated from high-resolution HiRISE images, at least three generations of alcoves can be distinguished. The inner slopes of Cilaos Crater preserve ancient erosional basins (fig. 12A), characterized by rounded edges and smooth morphology. These basins host smaller, better-preserved alcoves that are deeply incised by V-shaped channels. In contrast, the inner slopes of Gasa Crater contain the best-preserved and most recently formed alcove features (fig. 12B), which have sharp edges and a well-defined pinnate pattern. The size of the alcoves progressively decreases from the south-facing slopes to those facing west and east, a trend that is likely attributable to variations in solar insolation, with west- and east-facing

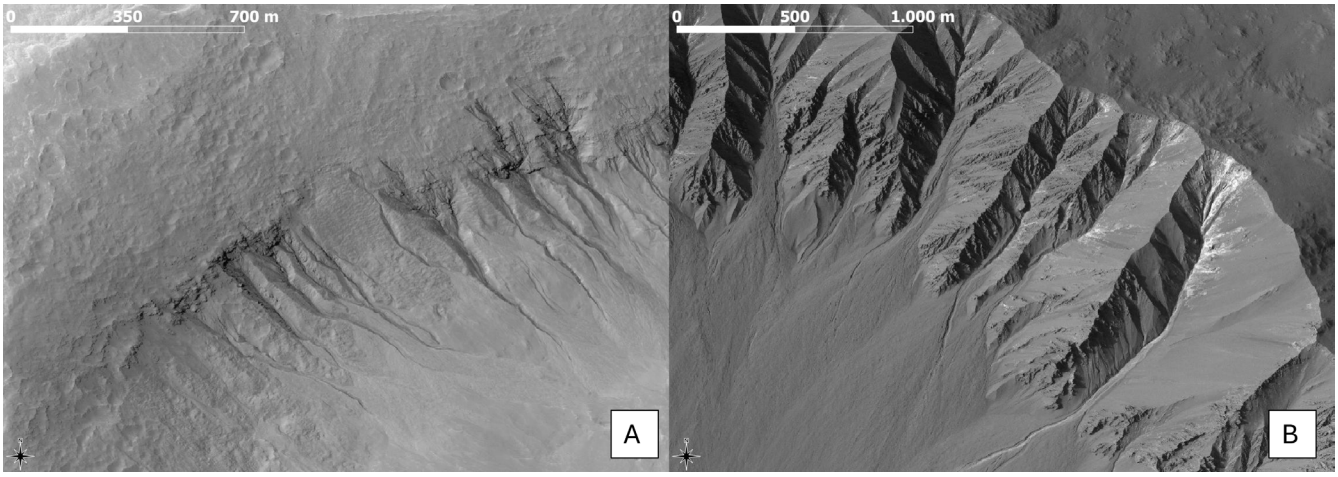

Figure 12 - Alcoves in the south-facing walls of Cilaos (A) and Gasa (B) Craters as seen in CTX P08_004060_1440_XI_36S230W.

slopes receiving less solar radiation than south-facing ones, thereby reducing the thermal energy available to drive sublimation-related geomorphic processes.

We identified four types of gullies based on their morphology: i) Classic gullies. These gullies consist of an eroded alcove, a V-shaped erosional channel, and a colluvial fan at the base of the slope, as first described by (Malin and Edgett (2000). Two examples of this type are found on the eastern wall of Cilaos Crater; ii) Complex gullies (sensu Auld and Dixon, 2016). These gullies feature morphologically complex alcoves, V-shaped channels, and depositional fans. They are termed "complex" because multiple alcoves converge into a single channel. The alcoves are broad upslope and narrow toward the channel. As with classic gullies, sediment transport appears to begin in the alcove, where material is incorporated into the flow; iii) Mantled gullies (Auld and Dixon, 2016). These gullies exhibit eroded and smooth alcoves covered by a fine, smooth mantle. Their channels are barely visible; iv) Channel gullies (Auld and Dixon, 2016). These gullies lack an alcove and may or may not develop an apron. Their primary function is as a channel. Channel gullies form within slope-mantling material and show no clear connection to the underlying bedrock or unconsolidated layers.

The network of alcove channels consists of a main V-shaped channel and multiple small tributary rills, forming a pinnate-like drainage basin. In the well-developed gully systems of Gasa Crater, sediment accumulation at the chute and base of the alcove can lead to channel backfilling. In these sediment-choked systems, channels tend to be discontinuous and braided. Additionally, some channels exhibit terraced cutbacks and, more rarely, levees. At the termini of the gullies, depositional lobes exhibit a light gray tone (fig. 13), a lobed morphology, and parallel linear structures aligned with the slope. Their dimensions vary, averaging approximately 300 m in length, with a slope of around 15°. These deposits accumulate to form cones that frequently extend beyond the channel margins, and in some cases, subsequent channel incision has partially reworked them. Additional morphologies may be ascribed to fluvial-like processes. Slightly convex, lobate deposits-interpreted as mudflow-related features-partially cover the crater floor (fig. 14). These deposits span an estimated area of approximately 1.109 km². On their surface, polygonal fracture patterns measuring roughly 127 m in width and 135 m in length are observable. The mudflow deposits are interconnected by short fluvial-like channels extending for ~200 m, which are infilled with fine-grained sediments subsequently reworked by aeolian activity, as evidenced by the presence of small transverse dunes (fig. 15).

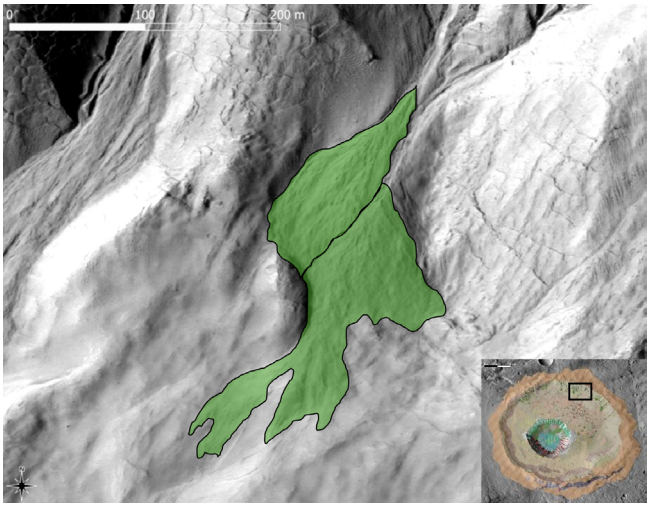

Figure 13 - Debris flow cones and lobes-like geomorphological features along the inner wall of the Cilaos Crater, as captured in HiRISE image ESP_011536_1440.

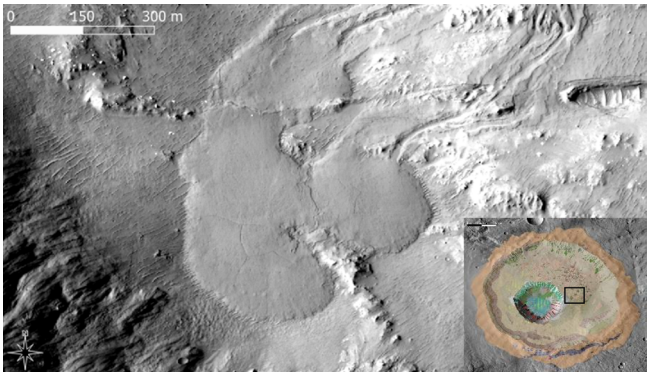

Figure 14 - Bilobate morphology of the mudflow deposit, which appears to be laterally displaced in a transverse direction (HiRISE image ESP_011536_1440).

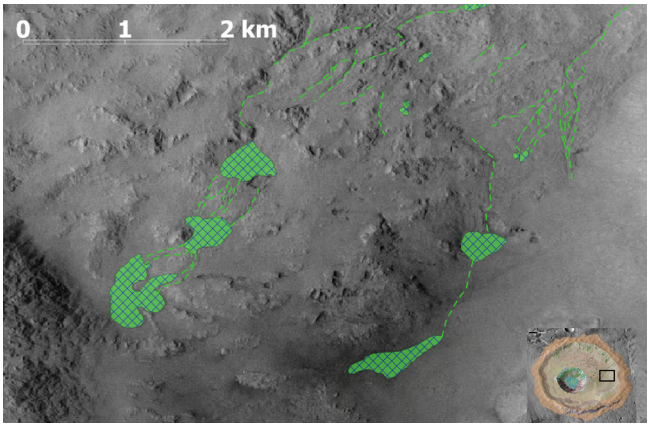

Figure 15 - Relationship between the mudflow deposits and the associated channel system (CTX image P08_004060_1440_XI_36S230W).

Complex landforms

Complex landforms are widespread within both Gasa and Cilaos craters. These morphologies are interpreted as the result of the interplay between multiple morphogenetic agents, including liquid water, gravity-driven processes, and aeolian activity.

A significant volume of material is deposited along the inner slopes of Gasa Crater, forming cone-shaped structures with variable geometries, dimensions, and slope angles. These deposits can be classified into two main types based on their slope inclination.

The first type, located along the southern inner wall of Gasa Crater, consists of a set of long, narrow debris cones with an average slope of approximately 35° and a mean length of ~800 m (fig. 16A).

In the lower portion of these deposits, polygenic cones with an average length of ~500 m are observed (fig. 16B). These cones display deeply incised surfaces, where the erosional features are organized into linear patterns aligned longitudinally with respect to the cone axis. Their average slope is approximately 25°.

The second type of deposit occurs along the northern inner wall of Gasa Crater (fig. 17). It comprises larger debris cones, with an average length of ~800 m and a mean slope of about 18°. These features are characterized by well-developed incision patterns and a markedly eroded surface.

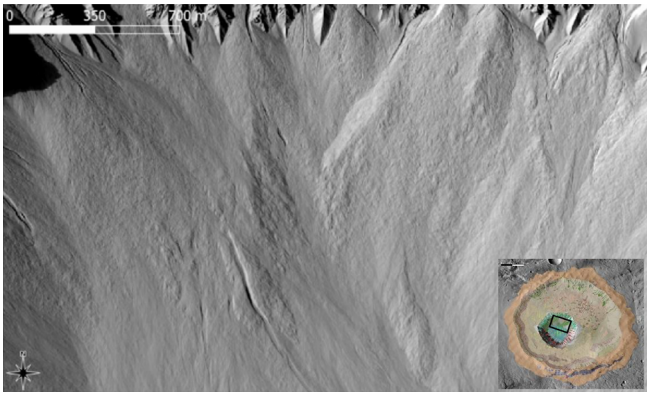

Figure 17 - Overview of polygenic deposits along the northern inner wall of Gasa Crater. Well-developed debris flow channel like landforms is indicated by the black arrow.

Within Cilaos Crater, a different type of complex landform is identified. The south-facing outer slope of the Cilaos Crater exhibits a suite of complex landforms organized into subparallel, step-like morphologies. These

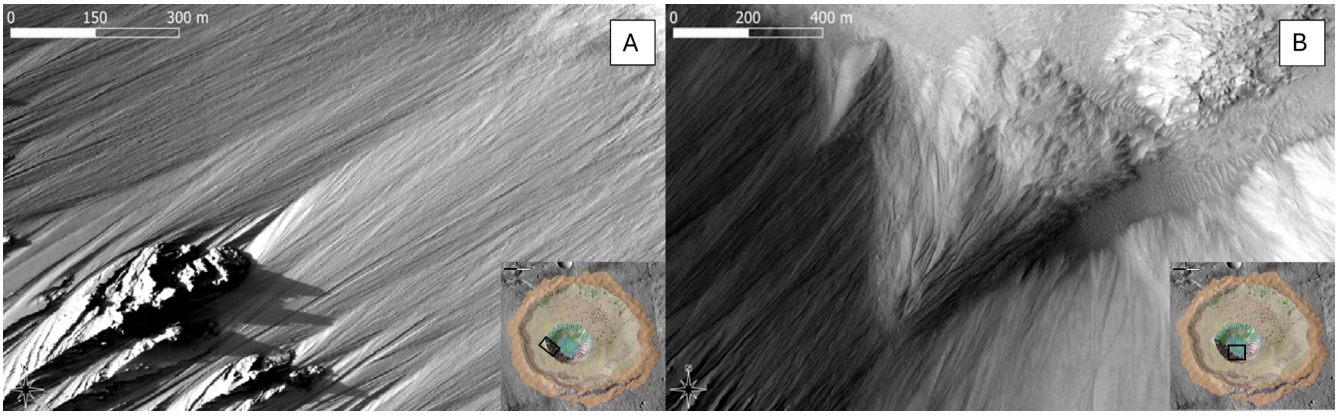

Figure 16 - A) Close-up view of deposits on the equator-facing wall of Gasa Crater (HiRISE ESP_020661_1440). B) Fan-shaped structure located on the same wall (HiRISE ESP_014147_1440).

morphologies are finely dissected by narrowly spaced, small-scale gullies oriented orthogonally to the slope steps and broadly parallel to one another. These irregularly shaped features (fig. 18), averaging ~20 m along their major axis, exhibit sharply defined boundaries and are interpreted as being associated with both structural and periglacial processes.

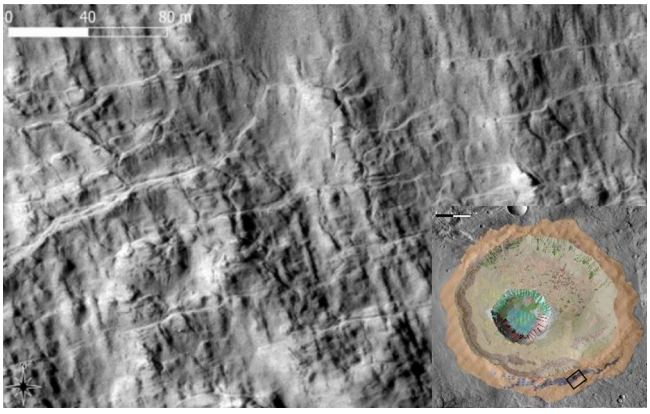

Figure 18 - Complex subparallel structures observed on the outer wall of Cilaos Crater.

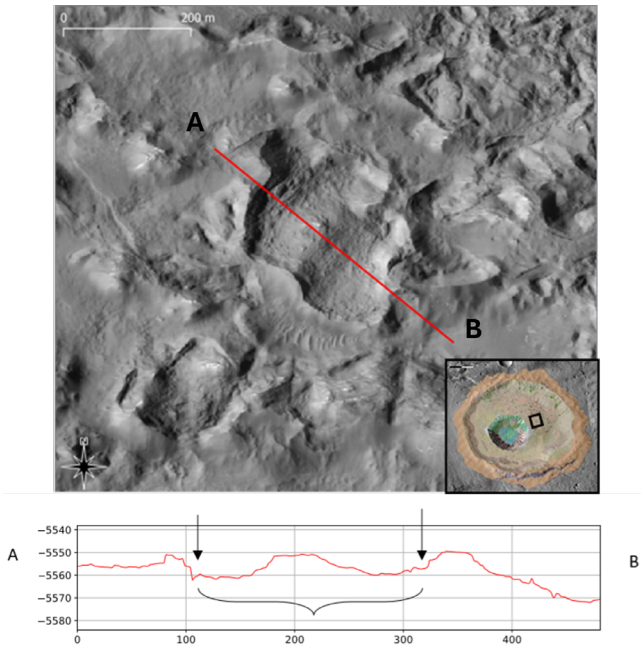

Figure 19 - Erosional window structures observed on the northeastern floor of Cilaos Crater.

Landforms of uncertain origin

In planetary geology, the interpretation of surface features is largely informed by analogues observed on Earth. Similar morphogenetic processes can produce comparable landforms, even when accounting for differing boundary conditions such as gravity, atmospheric pressure, and temperature. However, when surface morphologies lack a clear terrestrial analogue – particularly those that are highly complex or unfamiliar – constraining their genesis becomes significantly more challenging. This is the case for the following two landform types, which are herein classified as landforms of uncertain origin due to the absence of known terrestrial equivalents.

The first type is represented by the "erosional windows" (fig. 19), which are located on the northeastern floor of Cilaos Crater. They exhibit irregular morphologies and range in size from approximately 200 to 500 m in diameter. We refer to them as "erosional windows" due to their apparent exposure of the stratigraphically lowest units, suggesting a differential removal of overlying materials. A plausible hypothesis for their origin involves erosion and/or melting of the LDM, likely triggered by the Gasa impact event.

The margins of these features are characterized by stratified slopes and well-defined, sharp edges. The internal surfaces are rough and irregular, displaying a pattern of circular to subcircular bulged structures ranging from 5 to 15 m in diameter. These internal textures may indicate localized subsurface collapse, erosional processes, or other mechanisms not yet fully understood.

The second landform of uncertain origin is represented by "longitudinal tracks" (fig. 20), which are located along the pole-facing inner and outer walls of Cilaos Crater. These complex landforms are characterized by a series of parallel, linear incisions aligned downslope, forming a distinctive pattern of narrow, elongated grooves resembling the incised-Headwall Terrain described by Hubbard *et al.* (2011) Each groove is separated by sharp, straight ridges, with individual track widths ranging from approximately 5 to 50 m. At the base of these features, accumulations of fine-grained, smooth material are observed, likely resulting from mass-wasting processes, or sediment redistribution processes, i.e., water reworking of grooves.

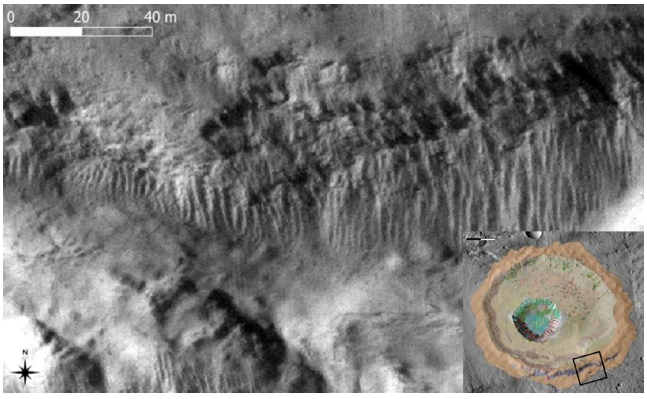

Figure 20 - Parallel longitudinal tracks developed on the pole-facing slopes of Cilaos Crater. Note the sharply defined ridges separating the grooves and the fine material accumulated at the base (HiRISE ESP_011536_1440_RED).

Structural landforms

These features, depicted on the geomorphological map (Supplementary Material) were delineated based on the alignment of various morphological indicators, including gully incisions, truncated flow lobes, channel segments, and portions of crater rims. Such patterns, composed of predominantly straight lineaments, are commonly observed in planetary terrains and are often indicative of underlying structural controls.

These features are interpreted as fractures or fault systems either induced by the impact event that formed Gasa Crater, or alternatively, they may reflect the reactivation of pre-existing crustal weaknesses. Notably, the rim of Gasa Crater exhibits a distinctly irregular, polygonal outline, resembling a near-hexagonal geometry. Several fractured segments of the rim are oriented parallel to the adjacent rim of Cilaos Crater, a relationship particularly evident in the western sectors of both structures.

PHOTOGEOLOGICAL UNITS

We identified 9 photogeological units in Cilaos Crater and 5 in Gasa Crater, depicted in the geomorphological and photogeological units map (Supplementary Material).

CILAOS' PHOTOGEOLOGICAL UNITS

Outer Wall Unit (OUTW)

This unit represents the outer rim of the Cilaos Crater (fig. 21). The unit displays light to dark grey tones and alternates between fine and coarse textures. In the southern area, small morphological features resembling organ pipes are present, while the remaining sections generally exhibit a more uniform pattern.

The crater rim appears significantly degraded and smoothed, with notable morphological variations along its perimeter. In the eastern sector (fig. 21B), the outer margin is characterized by light grey tones, a rough texture, and a series of linear features aligned with the slope gradient.

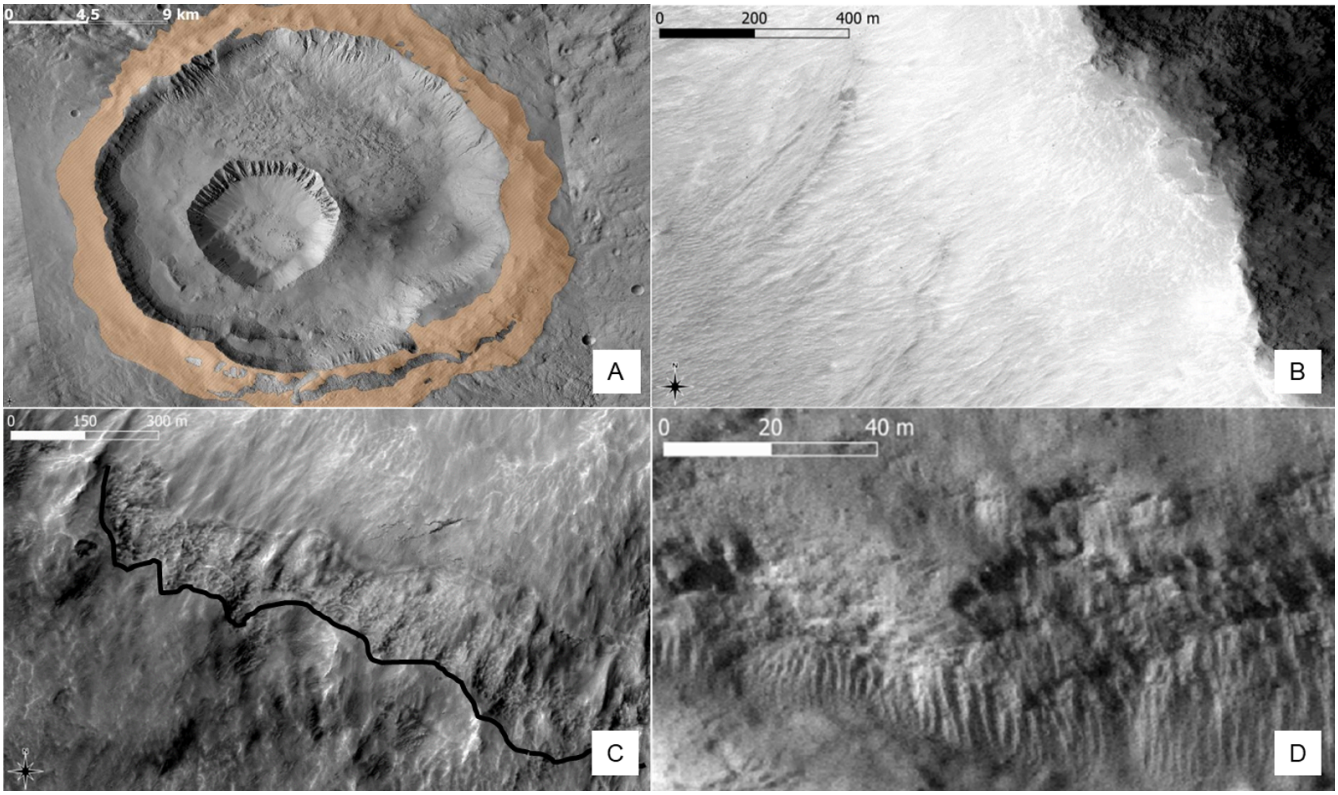

Figure 21 - A) Overview of the unit OUTW within the crater complex (CTX P08_004060_1440_XI_36S230W). B) Details of the eastern portion of the outer margin (HiRISE ESP_048458_1440_RED). C) Detail of the southern sector of the outer rim (HiRISE image ESP_011536_1440_RED). The black line delineates the erosional unconformity. The band exhibiting a coarser and rougher texture likely corresponds to the basal section of the slope, possibly consisting of bedrock that has undergone subsequent modification through periglacial processes. D) Example of the organ pipes, located in the southern outer rim of Cilaos.

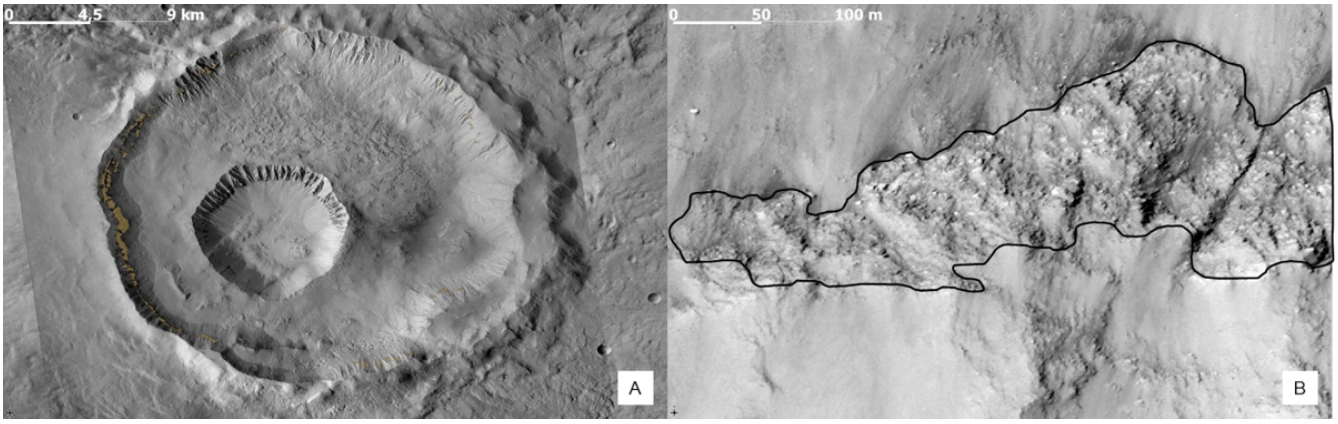

Figure 22 - A) The bedrock unit, located in the inner part of the rim (CTX P08_004060_1440_XI_36S230W). B) Detail of the unit (outlined by the black line), where the substrate exhibits an approximately parallel planar arrangement along the slope (HiRISE ESP_048458_1440).

Moving southward (fig. 21C), the morphology of the margin changes. The slope appears to be covered by fine-grained material, likely LDM, which in some areas reveals the underlying lower section – possibly the exposed bedrock.

Bedrock Unit (BED)

The BED unit (fig. 22A) exhibits a dark grey tone and a coarse surface texture. It is characterized by leopard-spot patterns and sub-parallel structures-oriented transverse to the slope, generally conforming to the curvature of the crater rim.

The linear arrangement of rock outcrops along the rim's outline (fig. 22B) suggests the presence of stratification, at least within the southern and southeastern sectors of the inner crater rim.

The *Bottom Units* (BOT) display a light to dark gray color (fig. 23) and a rough, coarse texture, with small subcircular structures exhibiting an irregular pattern. The surface is eroded and flattened, with the generally gentle slope locally interrupted by linear and pseudolinear structures. It could represent the Cilaos Crater floor, emerging for erosion/melting of the LDM as a consequence of Gasa impact.

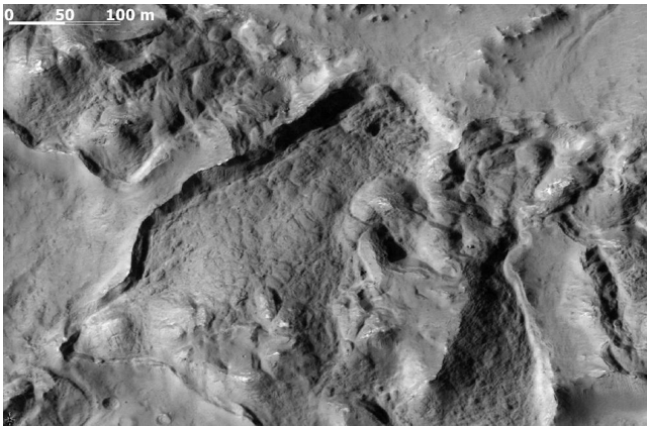

Figure 23 - Detailed view of the BOT unit, showing the rough texture and the small polygonal structure (HiRISE ESP_021584_1440).

Bedrock with Cover Unit (BEDC)

This unit is predominantly exposed in the northeastern sector of the Cilaos Crater floor, while in the southern portion it appears in isolated outcrops emerging from the southwestern inner wall deposit unit (fig. 24A). It displays a light grey to grey tone, influenced by local illumination conditions, and is characterized by a rough and coarse surface texture with fine, curvilinear and irregular morphological features. The unit would represent the remnant of the Gasa impact distal ejecta, covered by dust and other filling material.

This unit is predominantly exposed in the northeastern sector of the Cilaos Crater floor, while in the southern portion it appears in isolated outcrops emerging from the southwestern inner wall deposit unit (fig. 24B). It displays a light grey to grey tone, influenced by local illumination conditions, and is characterized by a rough and coarse surface texture with fine, curvilinear and irregular morphological features.

Densely Cratered Inner Wall Unit (CRA) exhibits a light grey to dark tone, a coarse surface texture, and irregularly distributed subcircular depressions. Within these depressions, fine-textured material is observed, interpreted as debris resulting from the degradation of the underlying substrate, along with coarser material, possibly ejecta (fig. 25).

North-Eastern Inner Wall Deposit Unit (NEU)

This photogeological unit displays a light to dark grey tonal range and is characterized by a coarse, rough texture. It contains a combination of linear and curvilinear features interspersed with isolated circular structures embedded within an irregular surface pattern. This unit appears to represent a transitional zone between the crater floor and the inner wall of Cilaos Crater (fig. 26A).

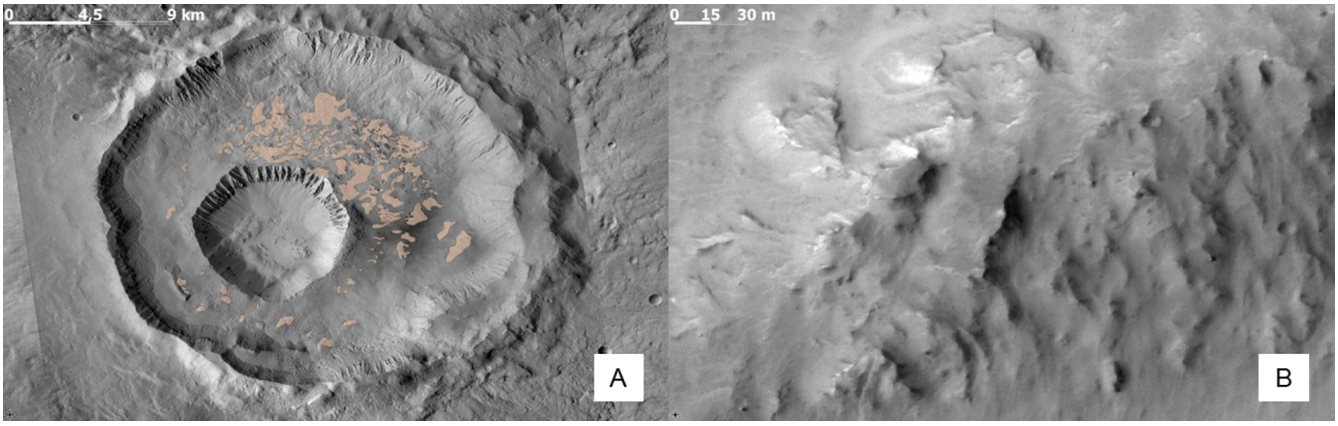

Figure 24 - A) BEDC unit location within the Cilaos floor (CTX P08_004060_1440_XI_36S230W). B) Sharp edge surrounded by thin material (ESP_011536_1440).

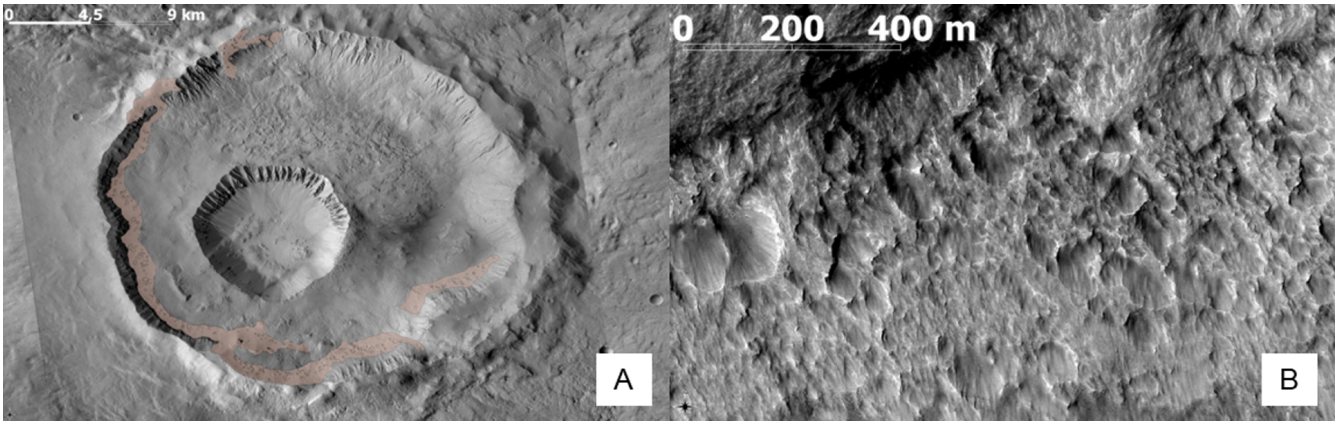

Figure 25 - A) CRA unit location in the complex crater (CTX P08_004060_1440_XI_36S230W). B) Detailed view of the Densely Cratered Inner Wall Unit, distinguished by high crater density and well-preserved circular morphologies (HiRISE ESP_048458_1440).

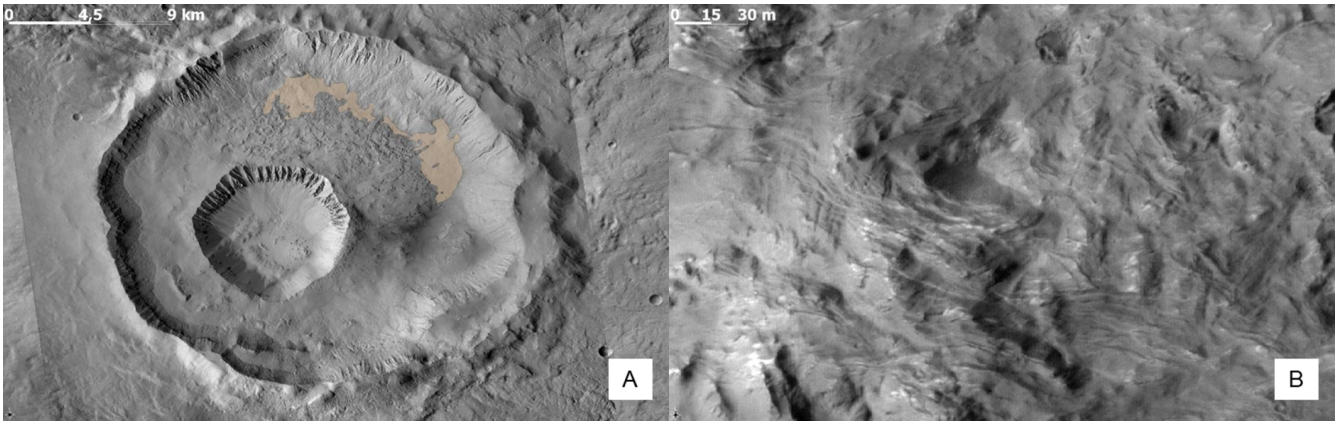

Figure 26 - A) The overview of the NEU unit in the northern part of the crater (CTX P08_004060_1440_XI_36S230W). B) Detail of some diffuse linear structures within the unit (HiRISE ESP_011536_1440).

The unit displays distinctive features that are clear only at HiRISE image resolutions. For instance, very small linear structures, exhibiting sinuous patterns and arranged in a non-systematic manner, can be clearly identified (fig. 26B).

South-Western Inner Wall Deposit Unit (SWU) displays tonal variations from light to dark grey and is characterized by a coarse, rough texture. It features linear structures elongated downslope, consistently oriented toward the interior of Gasa Crater, regardless of their specific

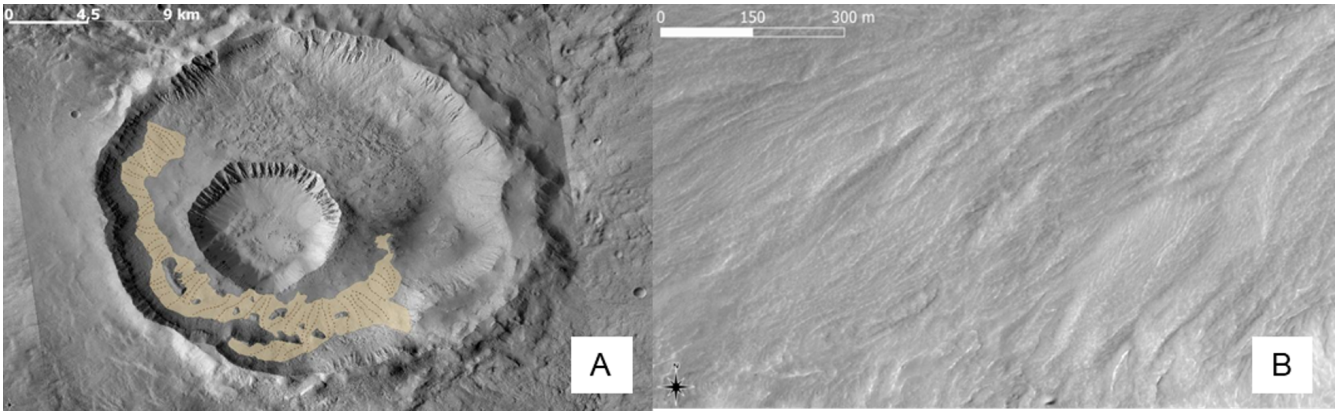

Figure 27 - A) Location of the SWU unit in the complex crater. B) Linear structures detail (HiRISE ESP_014147_1440).

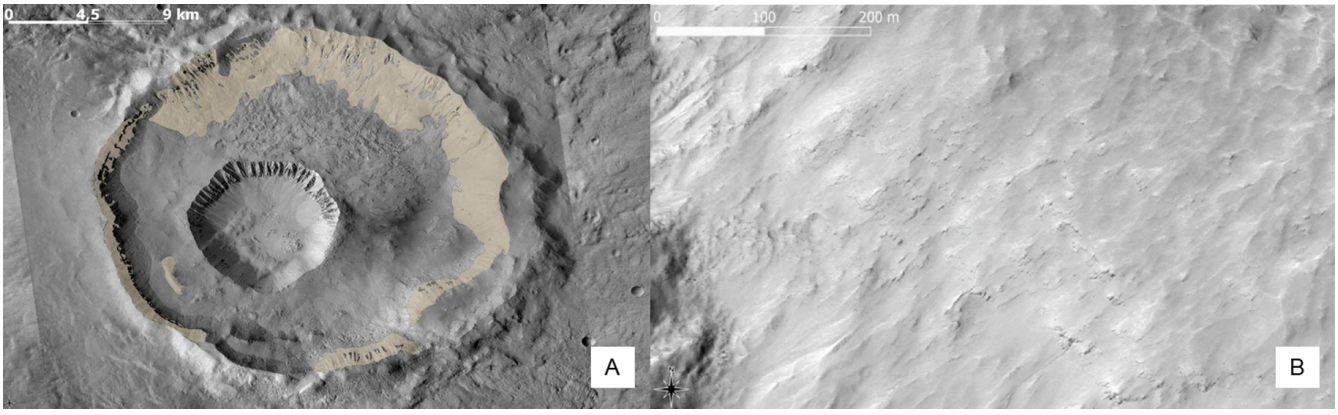

Figure 28 - A) Location of the INN unit within Cilaos (CTX P08_004060_1440_XI_36S230W). B) Detailed view of the unit (from HiRISE ESP_011536_1440).

geographic location. These linear features are overlain by small, irregularly shaped structures distributed across the unit surface (fig. 27). Their geometry and spatial pattern suggest features related to gravity-driven flows toward the inner crater, plausibly caused by post-impact mass wasting or reworking of ejecta.

Inner Wall Unit (INN)

This unit corresponds to the inner sector of the crater rim (fig. 28A). It is spatially extensive across the crater, with a more pronounced distribution in the northern portion than in the southern. The unit exhibits a tonal range from dark grey to light grey and is characterized by a coarse, irregular surface texture (fig. 28B). It displays elongated features aligned subparallel to the crater rim, and in some areas, leopard-like spotted patterns are visible near the uppermost part of the slope, adjacent to the rim crest. The unit is quite homogeneous, characterized by debris covers that accumulate along the slope.

Poligenic Filling Unit (POLC)

This unit is located on the Cilaos floor, where it is uniformly distributed (fig. 30A). Its density decreases slightly toward the southern sector of the floor. The unit exhibits a light gray to gray coloration, with an alternating pattern of rough and smooth surfaces. It is characterized by parallel linear structures and polygonal formations of metric scale dimensions (fig. 29B). It is likely that this unit represents the fill material of the Cilaos Crater floor, predominantly composed of dust, which has been extensively reworked by wind activity.

GASA' PHOTOGEOLOGICAL UNITS

Outer Wall Unit II (OUTII)

As the name suggests, this unit appears to be the remnant of the proximal ejecta outer rim of the Gasa Crater (fig. 30). It exhibits a gray to black coloration with a rough, coarse texture. Subcircular structures filled with fine-grained material are observed, encircled by parallel linear

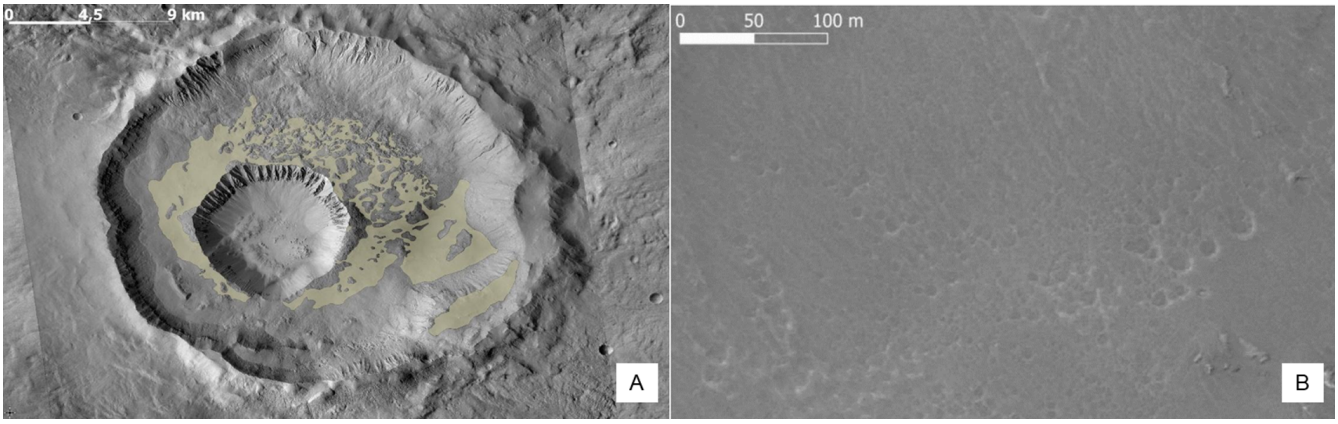

Figure 29 - A) The POLC unit location in the floor of Cilaos (CTX P08_004060_1440_XI_36S230W). B) Detailed view of the unit (HiRISE ESP_011536_1440).

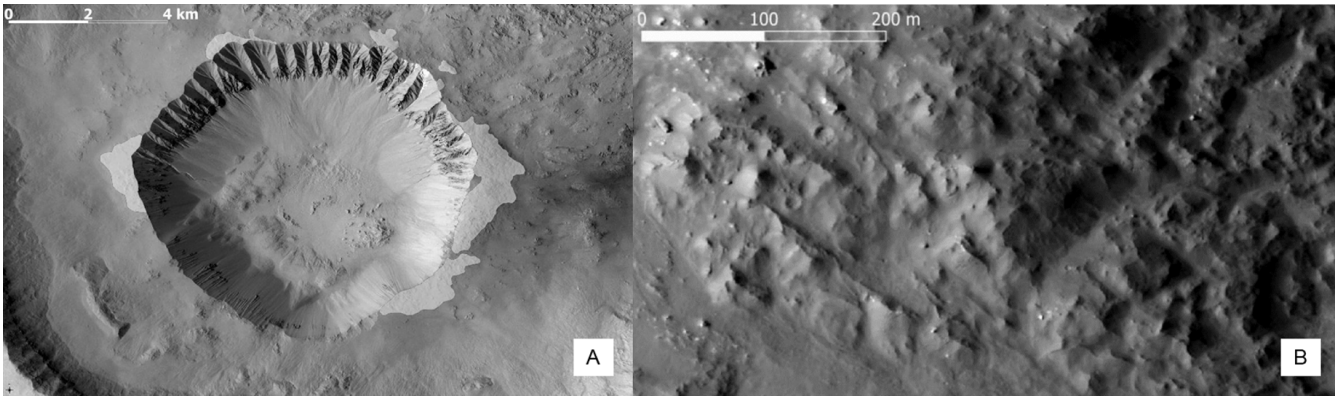

Figure 30 - A) The location of the OUTpp unit around Gasa Crater (CTX P08_004060_1440_XI_36S230W). B) Detail of the unit (HiRISE ESP_012024_1440).

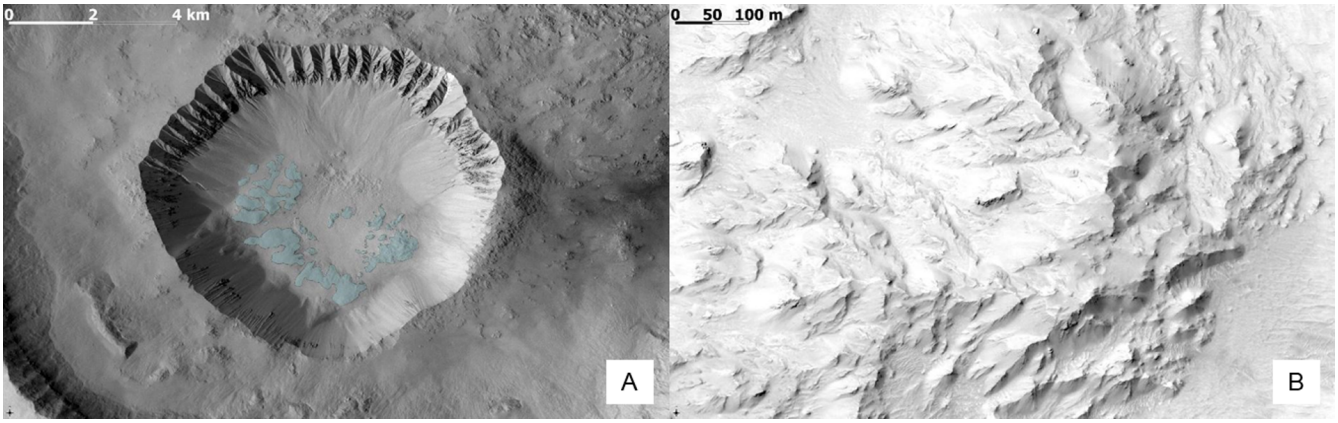

Figure 31 - A) The BEDF unit location on the floor of the Gasa Crater (CTX P08_004060_1440_XI_36S230W). B) Detail of the unit located in the eastern sector of the crater floor, characterized by sharper and more well-defined structures compared to the western portion (HiRISE ESP_021584_1440).

formations (fig. 30). The unit exhibits varying shades of gray in the eastern and western regions, influenced by differences in illumination

The unit exhibits varying shades of gray in the eastern and western regions, influenced by differences in illumination.

Floor-Bedrock Unit (BEDF)

The unit is situated at the base of Gasa Crater (fig. 31A) and exhibits two distinct morphological portions, differentiated by their degree of erosion. In the eastern sector, the unit displays an angular and sharply defined morphology (fig. 31B), whereas the remainder appears more eroded,

with a smoother surface texture. The unit exhibits tonal variations ranging from white to dark grey, and is characterized by a repetition of smooth and rough textures, as well as the presence of subcircular, irregularly distributed structures. This unit could be an impact breccia of the Gasa Crater impact event.

Poligenic Floor Unit (POLG)

The unit constitutes the infill material of the Gasa Crater floor (fig. 32A) and appears to have been shaped by aeolian processes. It exhibits light grey tonalities and a combination of smooth and rough surface textures, featuring polygonal structures of variable dimensions interspersed with linear features (fig. 32B).

Inner Wall Bedrock Unit (BEDW)

This unit exhibits a color range from dark grey to light grey and a coarse, rough texture. It is characterized by dendritic structures and leopard spots (fig. 33). This unit represents exposed substrate outcrops, which are arranged in leopard-like patches on the southern side, parallel to the crater edge. In contrast, the southeastern part shows no identified substrate outcrops, likely completely covered by slope debris.

Inner Wall-Bedrock with Cover Unit (BCW)

The photogeological unit is located within the inner rim of the Gasa Crater (fig. 34A), specifically occupying the pole-facing wall. Its shading ranges from dark to light gray, depending on slope illumination. The unit exhibits a fine, smooth texture and includes structures parallel to the crater rim, linear structures following the slope, and square-shaped formations.

The squared structures (fig. 35B), morphologically attributable to niches, exhibit a notable homogeneity. Specifically, they consist of a recurring pattern of structures aligned parallel to the crater rim at the highest elevation of the slope, which extends into longitudinal formations.

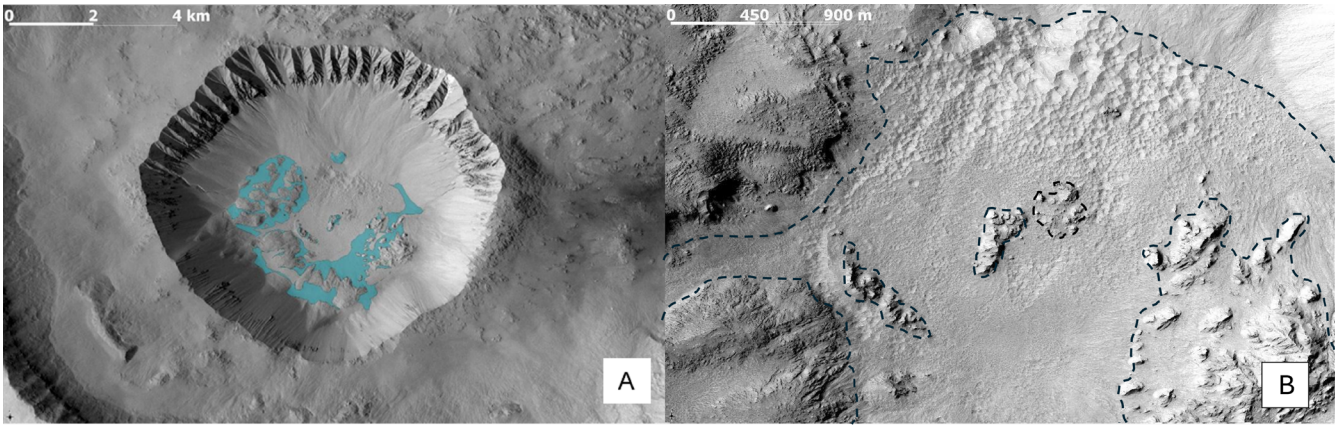

Figure 32 - A) Overview of the POLG unit in the floor of Gasa Crater (CTX P08_004060_1440_XI_36S230W). B) The dashed line outlined the polygenetic filling unit at the floor (HiRISE ESP_021584_1440).

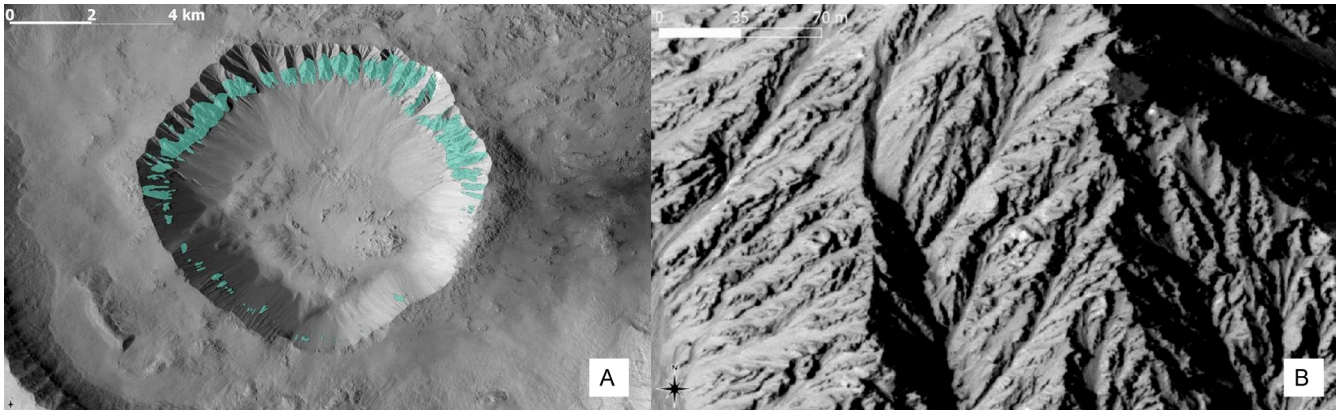

Figure 33 - A) Bedrock outcrops in the Gasa Crater. B) Focus on the bedrock outcrops (HiRISE ESP_021584_1440). These landforms are analogous to terrestrial badlands.

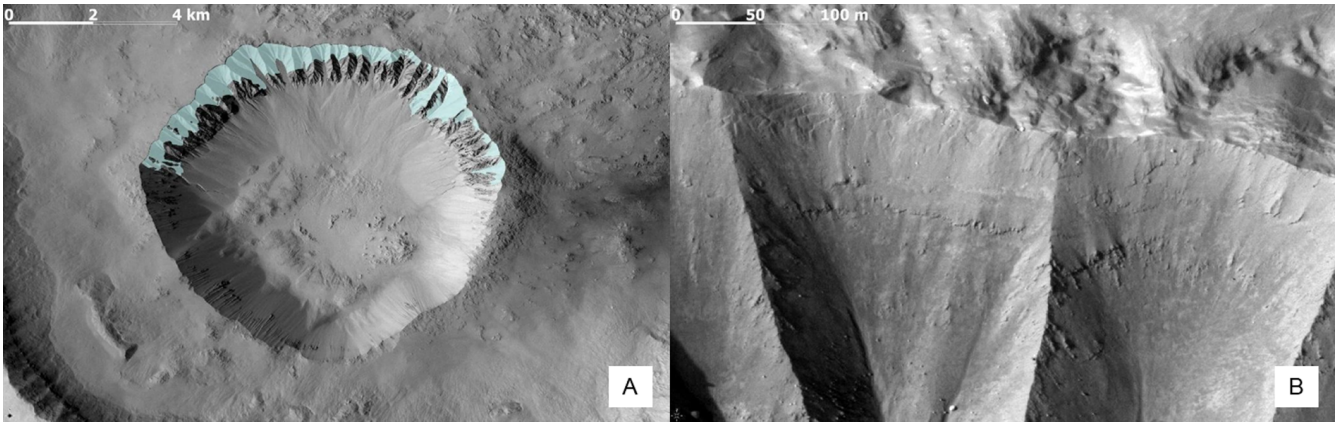

Figure 34 - A) Location of the BCW unit in the inner part of the Gasa Crater wall (CTX P08_004060_1440_XI_36S230W). B) Detail of the squared structures (HiRISE ESP_021584_1440).

DISCUSSION

With a diameter of 18 km, Cilaos Crater falls within the range of complex Martian craters. Despite the degradation made by LDM, Cilaos exhibits characteristic features of a complex crater with terraces and landslides along the inner wall (Hargitai and Öhman, 2015). Additionally, in the southeastern part of its inner rim, two large deep-seated gravitational slope deformations (DSGSDs) have developed, exhibiting a double rim. Similar structures have been observed on Mars, particularly in Valles Marineris (Kromuszczyńska *et al.*, 2019), where the formation of these features may be attributed to Marsquakes, meteoric impacts, or volcanic activity (Brunetti *et al.*, 2014).

Martian craters are generally affected by gravitational processes, occurring either during the collapse phase of the transient crater or in the post-impact stage. Our analysis reveals that the "Densely Cratered Inner Wall Unit", which we interpret as the result of interaction between Gasa's ejecta and the LDM, overlies the terraced surfaces of the DSGSDs. This suggests that the DSGSDs formed during the collapse phase of Cilaos' transient crater, consistent with the expected behavior of complex craters. Furthermore, Cilaos Crater lacks a central peak. According to the formula by Garvin *et al.* (2003) the central peak should have been approximately 175 m high. A combination of erosion and infilling processes likely contributed to its degradation. To evaluate infilling processes, we compared the depth-to-diameter (d/D) ratio of our craters with Martian trends identified by Robbins *et al.* 2018 (fig. 35). Cilaos crater's d/D value is slightly lower than expected, supporting the occurrence of modification events. Given the crater's latitude and evidence of degraded LDM, it is likely that LDM contributed to partial floor filling. However, since the estimated minimum thickness of LDM at mid-latitudes is ~10 m (Dickson *et al.*, 2015) insufficient to completely fill the crater floor-we infer that ejecta from the Gasa impact further contributed to its burial.

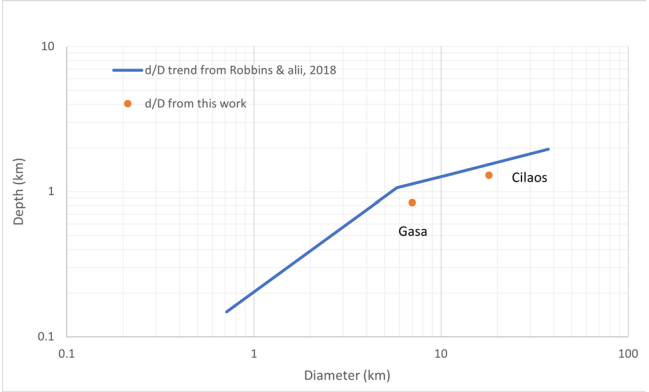

Figure 35 - Depth–diameter relation for the Cilaos and Gasa craters shown in logarithmic scale, alongside the empirical trend from Robbins *et al.* (2018).

Gasa Crater, with a diameter of ~7 km, is classified as a simple crater (Melosh, 1989; Hargitai and Watters, 2015), exhibiting no terraces or central peak. Its location near the simple-to-complex transition yet lying below the expected depth-to-diameter (d/D) trend (Fig. 35), is consistent with post-impact infilling or erosional degradation.

The contribution of LDM to this infilling is unlikely, as the impact appears to have occurred after the last deposition of mantled material. This is supported by the absence of LDM-related morphological features and the clear superposition of secondary craters and crater chains from Gasa on the LDM deposits (Garvin *et al.*, 2003; Schon and Head, 2012).

Gasa's floor is covered by fine aeolian sediments and mass-wasting deposits, including debris flows mantling its walls. THEMIS nighttime data analysis confirms the presence of fine sediments, as indicated by low thermal inertia values (Fergason *et al.*, 2006). The northern wall contains a significant accumulation of sediment organized into broad, eroded fan structures with slopes < 35°, suggesting a complex genesis involving gravity and possibly water activity. In contrast, the southern (equator-facing) wall exhibits

narrow, elongated fan-shaped deposits with slopes > 35°, indicative of predominantly gravitational processes. However, some cones along the southern wall have slopes < 15° (fig. 16), suggesting a possible water-related genesis. These deposits correspond to a large detachment niche at the crater's edge, implying that the cone material originated from ejecta (likely from the southwestern inner wall deposit unit) that fell back into the crater.

Starting from the outer wall of Cilaos, we observe "longitudinal tracks", frequently associated with dome-like structures (fig. 10). Similar features have been studied in Hellas Planitia (Hubbard *et al.*, 2011b) and attributed to water activity based on two key observations: (i) their alignment with slope trends, consistent with the behavior of water on inclined surfaces, and (ii) their uniform width, which suggests a non-gravitational origin (e.g., excluding boulder-induced erosion).

The fresh appearance of these incisions suggests relatively recent formation. If they are indeed water related in origin, we can eventually correlate them to pseudo-karst landforms. Possible water sources include near-surface ice (Costard *et al.*, 2002) or surface snow (Christensen, 2006). To further investigate, we analyzed HiRISE RGB images, which enhance terrain tone variations compared to grayscale imagery. Across different Martian seasons, a superficial patina (fig. 36) is observed covering large areas of the crater complex. Interpreted as a thin layer of H_2O and CO_2 deposited during winter, this patina would form as a consequence of extreme surface cooling on pole-facing slopes (Schorghofer and Edgett, 2006). The presence of this patina over the longitudinal incisions suggests a possible genesis linked to frost/sublimation cycles or even deliquescence phenomena.

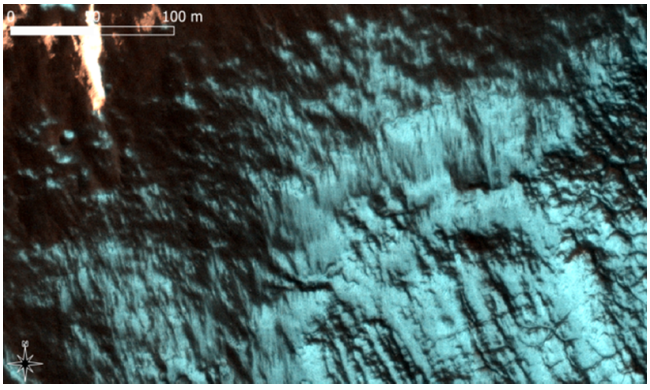

Figure 36 - HiRISE image PSP_009901_1440 illustrates the correlation between the presence of a white patina and longitudinal surface striations. The bluish hue of the patina is an artifact of image stretching, applied to enhance details in areas that remain in shadow. This patina is consistently observed in images acquired during the southern hemisphere's winter, suggesting a seasonal occurrence. It is notably absent in autumn images, and although summer data are lacking for this region, the absence of the patina in spring imagery further supports its confinement to the colder months.

Below the incisions, we observe polygonal terrain resembling terrestrial patterned ground, similar to features identified elsewhere on Mars where LDM has been dissected (Mangold, 2005). This terrain is typically associated with periglacial processes and would document freeze-thaw cycles.

Both craters exhibit pole-facing gullies. Cilaos displays three generations of gullies, with the earliest forming well defined alcove in the inner wall. These were later partially obscured by a second generation of gullies. The most recent generation consists of shallower, shorter gullies (~270 m in length), likely representing the most recent activity. Similar features have been studied in Antarctica's McMurdo Dry Valleys, one of Earth's driest and coldest regions. Hauber *et al.* (2019) examined potential water sources for Antarctic gullies, typically associated with rainfall-triggered debris flows. However, as in the Martian mid-latitudes, rain is absent in Antarctica, meaning ice or snowmelt must be responsible. While air temperatures rarely exceed 0° C, rock temperatures can rise above the melting point, especially in low-albedo areas (Hauber *et al.*, 2019).

On Mars, snow is absent at these latitudes, leaving subsurface ice as the most plausible water source. Previous studies suggest LDM could supply water for gully formation in mid-latitudes (Head *et al.*, 2003, 2008; Bleamaster and Crown, 2005; Bridges and Lackner, 2006; Dickson and Head, 2009). Given the known degradation of LDM in Cilaos Crater, it is reasonable to infer that Gasa Crater impacted an ice-rich substrate, triggering localized ice melting and subsequent gully formation (Schon and Head, 2012). However, recent observations by Dundas *et al.* (2010) suggest that some gully modifications are driven by dry processes rather than liquid water activity attributed to exposure and sublimation of ice or rockfalls as observed in Gasa Crater.

On Cilaos' Crater walls, small-scale polygonal features have been identified within gully-affected areas (fig. 10). Similar structures have been observed in nearby craters, suggesting their formation is unrelated to the Gasa impact. These features, referred to as "gully polygons" or "gully-gons" are classified as composite wedge polygons, indicative of episodic water presence likely linked to gully activity (Levy *et al.*, 2009).

Gravity remains the dominant morphogenetic agent in both craters. Cilaos' inner walls exhibit slope-transverse fractures resembling trenches, possibly formed by the Gasa impact. The western slopes of Gasa Crater display numerous rockfalls, with some showing visible boulder paths (fig. 8). Several detachment niches have been mapped along the walls of Cilaos, unrelated to water activity, as no incisions lead to debris fans. These gravitational processes likely postdate the Gasa impact, as slope debris covers remnants of the impact craters within the "Densely Cratered Inner Wall Unit" (fig. 26B).

CONCLUSION

The landscape analysis allowed for a detailed characterization of the landforms and deposits within the study area. Each feature was described and interpreted based on terrestrial analogues and Martian literature. This approach enabled the identification of three dominant morphogenetic agents responsible for shaping the crater complex after the impact: gravity, wind, and possibly water, in the form of meltwater from subsurface ice.

A geomorphological map at a scale of 1:25,000 was produced, accompanied by a legend delineating photogeological units (9 for the Cilaos Crater and 5 for the Gasa Crater) and landforms, categorized as either "Landforms associated with a specific morphogenesis" or "Complex landforms with uncertain origin." This map effectively represents the spatial distribution of the landforms within the study area, providing a comprehensive and immediate understanding of the relationships between individual structures and their distribution within the crater complex.

While the analysis of individual landforms is useful for morphological description, their broader spatial and contextual relationships are crucial for a more holistic interpretation. The geomorphological map fulfils this need, allowing for a better assessment of the distribution of features such as gullies, rockfalls, and secondary impact craters. In some cases, identifying a specific morphogenetic agent was not entirely clear. While certain features exhibit similarities to terrestrial morphologies, the precise processes responsible for their formation remain uncertain. Additionally, establishing a precise relative chronology was challenging due to unclear relationships between landforms and surface deposits.

The findings of this study contribute to the broader understanding of Martian surface evolution, particularly in mid-latitude cratered terrains. The presence of well-developed gullies and possible periglacial features supports the hypothesis of past ice-related processes, consistent with previous studies on similar regions of Mars. Moreover, the observed evidence of mass wasting, rockfalls, and secondary impact structures highlights the complexity of post-impact modifications, emphasizing the role of both gravitational and aeolian processes in shaping the Martian landscape over time.

Future research may address these uncertainties by leveraging advancements in available data, including higher-resolution imagery, improved topographic data, and additional in situ observations from Mars rovers. Comparative studies of craters at similar latitudes could also provide valuable insights, helping to refine interpretations of the processes that have shaped the Martian surface over time. Furthermore, numerical modeling and experimental simulations of slope processes under Martian conditions could provide a more quantitative understanding of the mechanisms driving the observed geomorphological features. Finally, the integration of remote sensing, field analogue studies on Earth, and numerical modelling will be essential for advancing our knowledge of the geological history and climatic evolution of Mars.

SUPPLEMENTARY MATERIAL

Supplementary material, including the "Geomorphological and Photogeological Units Map of Cilaos Crater: Interpretation of Landforms and Surface Processes in Eastern Promethei Terra, Mars" at the scale of 1:50,000, associated to this article can be found in the on-line version at https://doi.org/10.4454/gtr56snb

AUTHORS CONTRIBUTION

SB, MCS, AP and CB conducted photogeological and remote sensed analysis; SB, MCS, CB realized the geomorphological map; SB and MCS wrote the paper with the contribute of all the Authors; CB conceived the work and found financial support.

ACKNOWLEDGMENTS

This work was conducted in the framework of the "SPaceItUp Project" funded by ASI (Italian Space Agency) and by MUR (Ministry of University and Research), under contract n. 2024-5-E.0 - CUP n. I53D24000060005 and of INAF MINI-GRANTS (2024) "Multi-approach analysis on Martian and terrestrial rock glaciers: paleoclimatic implications and evaluation of permafrost behaviour" (C93C24008060001).
We sincerely wish to thank two Anonymous Reviewers for their constructive comments and insightful suggestions, which have greatly contributed to improving the quality of this manuscript.

REFERENCES

Auld K.S., Dixon J.C., 2016. *A classification of martian gullies from HiRISE imagery*. Planetary and Space Science, 131, 88-101. https://doi.org/10.1016/j.pss.2016.08.002

Balme M., Mangold N., Baratoux D., Costard F., Gosselin M., Masson P., Pinet P., Neukum G., 2006. *Orientation and distribution of recent gullies in the southern hemisphere of Mars: observations from High Resolution Stereo Camera/Mars Express (HRSC/MEX) and Mars Orbiter Camera/Mars Global Surveyor (MOC/MGS) data*. Journal of Geophysical Research: Planets, 111 (E5), 2005JE002607. https://doi.org/10.1029/2005JE002607

Beyer R.A., Alexandrov O., McMichael S., 2018. *The Ames Stereo Pipeline: NASA's Open Source Software for Deriving and Processing Terrain Data*. Earth and Space Science, 5 (9), 537-548. https://doi.org/10.1029/2018EA000409

Bleamaster L.F., Crown D.A., 2005. *Mantle and gully associations along the walls of Dao and Harmakhis Valles, Mars*. Geophysical Research Letters, 32 (20), 2005GL023548. https://doi.org/10.1029/2005GL023548

Bridges N.T., Lackner C.N., 2006. *Northern hemisphere Martian gullies and mantled terrain: Implications for near-surface water migration in Mars' recent past*. Journal of Geophysical Research: Planets, 111 (E9), 2006JE002702. https://doi.org/10.1029/2006JE002702

Brunetti M.T., Guzzetti F., Cardinali M., Fiorucci F., Santangelo M., Mancinelli P., Komatsu G., Borselli L., 2014. *Analysis of a new geomorphological inventory of landslides in Valles Marineris, Mars*. Earth and Planetary Science Letters, 405, 156-168. https://doi.org/10.1016/j.epsl.2014.08.025

Campobasso C., Carton A., Chelli M., D'Orefice M., Dramis F., Graciotti R., Guida D., Pambianchi G., Peduto F., Pellegrini L., 2018. *Aggiornamento ed integrazioni delle linee guida della carta geomorfologica d'Italia alla scala 1:50.000. Carta geomorfologica d'Italia-1:50.000.* ISPRA - Istituto Superiore per la Protezione e Ricerca Ambientale, 95 pp.

Christensen P.R., 2006. *Water at the Poles and in Permafrost Regions of Mars*. Elements, 2 (3), 151-155. https://doi.org/10.2113/gselements.2.3.151

Conway S.J., Balme M.R., Kreslavsky M.A., Murray J.B., Towner M.C., 2015. *The comparison of topographic long profiles of gullies on Earth to gullies on Mars: A signal of water on Mars*. Icarus, 253, 189-204. https://doi.org/10.1016/j.icarus.2015.03.009

Conway S.J., Harrison T.N., Soare R.J., Britton A.W., Steele L.J., 2019. *New slope-normalized global gully density and orientation maps for Mars*. Geological Society, London, Special Publications, 467 (1), 187-197. https://doi.org/10.1144/SP467.3

Costard F., Forget F., Mangold N., Peulvast J.P., 2002. *Formation of recent Martian debris flows by melting of near-surface ground ice at high obliquity*. Science, 295 (5552), 110-113. https://doi.org/10.1126/science.1066698

Della Seta M., Esposito C., Marmoni G.M., Martino S., Scarascia Mugnozza G., Troiani F., 2017. *Morpho-structural evolution of the valley-slope systems and related implications on slope-scale gravitational processes: new results from the Mt. Genzana case history (Central Apennines, Italy)*. Geomorphology, 289, 60-77. https://doi.org/10.1016/j.geomorph.2016.07.003

Dickson J.L., Head J.W., 2009. *The formation and evolution of youthful gullies on Mars: gullies as the late-stage phase of Mars' most recent ice age*. Icarus, 204 (1), 63-86. https://doi.org/10.1016/j.icarus.2009.06.018

Dickson J.L., Head J.W., Goudge T.A., Barbieri L., 2015. *Recent climate cycles on Mars: stratigraphic relationships between multiple generations of gullies and the latitude dependent mantle*. Icarus, 252, 83-94. https://doi.org/10.1016/j.icarus.2014.12.035

Diniega S., Byrne S., Bridges N.T., Dundas C.M., McEwen A.S., 2010. *Seasonality of present-day Martian dune-gully activity*. Geology, 38 (11), 1047-1050. https://doi.org/10.1130/G31287.1

Discenza M.E., Esposito C., Komatsu G., Miccadei E., 2021. *Large-scale and deep-seated gravitational slope deformations on Mars: a review*. Geosciences, 11 (4), 174. https://doi.org/10.3390/geosciences11040174

Dramis F., Sorriso-Valvo M., 1994. *Deep-seated gravitational slope deformations, related landslides and tectonics*. Engineering Geology, 38 (3-4), 231-243. https://doi.org/10.1016/0013-7952(94)90040-X

Dundas C.M., McEwen A.S., Diniega S., Byrne S., Martinez-Alonso S., 2010a. *New and recent gully activity on Mars as seen by HiRISE*. Geophysical Research Letters, 37 (7), 2009GL041351. https://doi.org/10.1029/2009GL041351

Dundas C.M., McEwen A.S., Diniega S., Byrne S., Martinez-Alonso S., 2010b. *New and recent gully activity on Mars as seen by HiRISE*. Geophysical Research Letters, 37 (7), 2009GL041351. https://doi.org/10.1029/2009GL041351

Dundas C.M., McEwen A.S., Chojnacki M., Milazzo M.P., Byrne S., McElwaine J.N., Urso A., 2017. *Granular flows at recurring slope lineae on Mars indicate a limited role for liquid water*. Nature Geoscience, 10 (12), 903-907. https://doi.org/10.1038/s41561-017-0012-5

Fergason R.L., Christensen P.R., Kieffer H.H., 2006. *High-resolution thermal inertia derived from the Thermal Emission Imaging System (THEMIS): thermal model and applications*. Journal of Geophysical Research: Planets, 111 (E12), 2006JE002735. https://doi.org/10.1029/2006JE002735

Garvin J.B., Sakimoto S.E.H., Frawley J.J., 2003. *Craters on Mars: Global Geometric Properties from Gridded MOLA Topography*, Lunar and Planetary Institute, Pasadena, US Sixth International Conference on Mars, 1-3.

Hartmann W.K., 2005. *Martian cratering 8: isochron refinement and the chronology of Mars.* Icarus, 174, 294-320. https://doi.org/10.1016/j.icarus.2004.11.023

Hargitai H., Öhman T., 2015. *Complex Crater*. In: Hargitai H., Kereszturi Á. (Eds), Encyclopedia of Planetary Landforms, 340-353. Springer, New York. https://doi.org/10.1007/978-1-4614-3134-3_429

Hargitai H., Watters W.A., 2015. *Simple crater*. In: Hargitai H., Kereszturi Á. (Eds), Encyclopedia of Planetary Landforms, 1939-1946. Springer, New York. https://doi.org/10.1007/978-1-4614-3134-3

Hauber E., Sassenroth C., De Vera J.-P., Schmitz N., Jaumann R., Reiss D., Hiesinger H., Johnsson A., 2019. *Debris flows and water tracks in northern Victoria Land, continental East Antarctica: a new terrestrial analogue site for gullies and recurrent slope lineae on Mars*. Geological Society, London, Special Publications, 467 (1), 267-287. https://doi.org/10.1144/SP467.12

Head J.W., Mustard J.F., Kreslavsky M.A., Milliken R.E., Marchant D.R., 2003. *Recent ice ages on Mars*. Nature, 426 (6968), 797-802. https://doi.org/10.1038/nature02114

Head J.W., Marchant D.R., Kreslavsky M.A., 2008. *Formation of gullies on Mars: link to recent climate history and insolation microenvironments implicate surface water flow origin*. Proceedings of the National Academy of Sciences, 105 (36), 13258-13263. https://doi.org/10.1073/pnas.0803760105

Hobbs S.W., Paull D.J., Clarke J.D.A., 2017. *Testing the water hypothesis: quantitative morphological analysis of terrestrial and martian mid-latitude gullies*. Geomorphology, 295, 705-721. https://doi.org/10.1016/j.geomorph.2017.08.021

Hubbard B., Milliken R.E., Kargel J.S., Limaye A., Souness C., 2011a. *Geomorphological characterisation and interpretation of a mid-latitude glacier-like form: Hellas Planitia, Mars*. Icarus, 211 (1), 330-346. https://doi.org/10.1016/j.icarus.2010.10.021

Hubbard B., Milliken R.E., Kargel J.S., Limaye A., Souness C., 2011b. *Geomorphological characterisation and interpretation of a mid-latitude glacier-like form: Hellas Planitia, Mars*. Icarus, 211 (1), 330-346. https://doi.org/10.1016/j.icarus.2010.10.021

Jaumann R., Neukum G., Behnke T., Duxbury T.C., Eichentopf K., Flohrer J., Gasselt S. v., Giese B., Gwinner K., Hauber E., Hoffmann H., Hoffmeister A., Köhler U., Matz K.-D., McCord T.B., Mertens V., Oberst J., Pischel R., Reiss D., Ress E., Roatsch T., Saiger P., Scholten F., Schwarz G., Stephan K., Wählisch M., 2007. *The high-resolution stereo camera (HRSC) experiment on Mars Express: instrument aspects and experiment conduct from interplanetary cruise through the nominal mission*. Planetary and Space Science, 55 (7-8), 928-952. https://doi.org/10.1016/j.pss.2006.12.003

Jouannic G., Conway S.J., Gargani J., Costard F., Massé M., Bourgeois O., Carter J., Schmidt F., Marmo C., Ori G.G., Nachon M., Pasquon K., 2019. *Morphological characterization of landforms produced by*

springtime seasonal activity on Russell Crater megadune, Mars. Geological Society Special Publication, 467 (1), 115-144. https://doi.org/10.1144/SP467.16

Kreslavsky M.A., Head J.W., 2002. *Mars: Nature and evolution of young latitude-dependent water-ice-rich mantle*. Geophysical Research Letters, 29 (15). https://doi.org/10.1029/2002GL015392

Kromuszczyńska O., Mège D., Dębniak K., Gurgurewicz J., Makowska M., Lucas A., 2019. *Deep-seated gravitational slope deformation scaling on Mars and Earth: same fate for different initial conditions and structural evolutions*. Earth Surface Dynamics, 7 (2), 361-376. https://doi.org/10.5194/esurf-7-361-2019

Lagain A., Bouley S., Zanda B., Miljković K., Rajšić A., Baratoux D., Payré V., Doucet L.S., Timms N.E., Hewins R., Benedix G.K., Malarewic V., Servis K., Bland P.A., 2022. *Early crustal processes revealed by the ejection site of the oldest martian meteorite*. Nature Communications, 13 (1), 3782. https://doi.org/10.1038/s41467-022-31444-8

Levy J., Head J., Marchant D., 2009. *Thermal contraction crack polygons on Mars: classification, distribution, and climate implications from HiRISE observations*. Journal of Geophysical Research: Planets, 114 (E1), 2008JE003273. https://doi.org/10.1029/2008JE003273

Levy J.S., Head J.W., Marchant D.R., Kowalewski D.E., 2008. *Identification of sublimation-type thermal contraction crack polygons at the proposed NASA Phoenix landing site: implications for substrate properties and climate-driven morphological evolution*. Geophysical Research Letters, 35 (4), L04202. https://doi.org/10.1029/2007GL032813

Malin M.C., Edgett K.S., 2000. *Evidence for recent groundwater seepage and surface runoff on Mars*. Science, 288 (5475), 2330-2335. https://doi.org/10.1126/science.288.5475.2330

Malin M.C., Bell J.F., Cantor B.A., Caplinger M.A., Calvin W.M., Clancy R.T., Edgett K.S., Edwards L., Haberle R.M., James P.B., Lee S.W., Ravine M.A., Thomas P.C., Wolff M.J., 2007. *Context Camera Investigation on board the Mars Reconnaissance Orbiter*. Journal of Geophysical Research: Planets, 112 (E5), 2006JE002808. https://doi.org/10.1029/2006JE002808

Mangold N., 2005. *High latitude patterned grounds on Mars: classification, distribution and climatic control*. Icarus, 174 (2), 336-359. https://doi.org/10.1016/j.icarus.2004.07.030

Mangold N., Mangeney A., Migeon V., Ansan V., Lucas A., Baratoux D., Bouchut F., 2010. *Sinuous gullies on Mars: frequency, distribution, and implications for flow properties*. Journal of Geophysical Research: Planets, 115 (E11), 2009JE003540. https://doi.org/10.1029/2009JE003540

McEwen A.S., Eliason E.M., Bergstrom J.W., Bridges N.T., Hansen C.J., Delamere W.A., Grant J.A., Gulick V.C., Herkenhoff K.E., Keszthelyi L., Kirk R.L., Mellon M.T., Squyres S.W., Thomas N., Weitz C.M., 2007. *Mars Reconnaissance Orbiter's High Resolution Imaging Science Experiment (HiRISE)*. Journal of Geophysical Research: Planets, 112 (E5), 2005JE002605. https://doi.org/10.1029/2005JE002605

Melosh H.J., 1989. *Impact cratering: a geologic process*. Oxford Monographs on Geology and Geophysics Series, 11. Clarendon Press, Oxford, 245 pp.

Miyamoto H., Dohm J.M., Baker V.R., Beyer R.A., Bourke M., 2004. *Dynamics of unusual debris flows on Martian sand dunes*. Geophysical Research Letters, 31 (13), 2004GL020313. https://doi.org/10.1029/2004GL020313

Neukum G., Jaumann R., 2004. *HRSC: the High Resolution Stereo Camera on Mars Express*. In: Chicarro A. (Ed.), Mars Express: the scientific payload; [a European mission to the Red Planet], 17-35. ESA Publications Division, Noordwijk.

Pasquon K., Gargani J., Massé M., Conway S.J., 2016. *Present-day formation and seasonal evolution of linear dune gullies on Mars*. Icarus, 274, 195-210. https://doi.org/10.1016/j.icarus.2016.03.024

Peulvast J.-P., Mège D., Chiciak J., Costard F., Masson P.L., 2001. *Morphology, evolution and tectonics of Valles Marineris wallslopes (Mars)*. Geomorphology, 37 (3-4), 329-352. https://doi.org/10.1016/S0169-555X(00)00085-4

Raack J., Reiss D., Appéré T., Vincendon M., Ruesch O., Hiesinger H., 2015. *Present-day seasonal gully activity in a south polar pit (Sisyphi Cavi) on Mars*. Icarus, 251, 226-243. https://doi.org/10.1016/j.icarus.2014.03.040

Reiss D., Hiesinger H., Hauber E., Gwinner K., 2009. *Regional differences in gully occurrence on Mars: a comparison between the Hale and Bond craters*. Planetary and Space Science, 57 (8–9), 958–974. https://doi.org/10.1016/j.pss.2008.09.008

Robbins S.J., Riggs J.D., Weaver B.P., Bierhaus E.B., Chapman C.R., Kirchoff M.R., Singer K.N., Gaddis L.R., 2018. *Revised recommended methods for analyzing crater size-frequency distributions*. Meteoritics & Planetary Science, 53 (4), 891-931. https://doi.org/10.1111/maps.12990

Schon S.C., Head J.W., Fassett C.I., 2009. *Unique chronostratigraphic marker in depositional fan stratigraphy on Mars: evidence for ca. 1.25 Ma gully activity and surficial meltwater origin*. Geology, 37 (3), 207-210. https://doi.org/10.1130/G25398A.1

Schon S.C., Head J.W., 2011. *Keys to gully formation processes on Mars: Relation to climate cycles and sources of meltwater*. Icarus, 213 (1), 428-432. https://doi.org/10.1016/j.icarus.2011.02.020

Schon S.C., Head J.W., 2012. *Gasa impact crater, Mars: very young gullies formed from impact into latitude-dependent mantle and debris-covered glacier deposits?*. Icarus, 218 (1), 459-477. https://doi.org/10.1016/j.icarus.2012.01.002

Schorghofer N., Edgett K.S., 2006. *Seasonal surface frost at low latitudes on Mars*. Icarus, 180 (2), 321-334. https://doi.org/10.1016/j.icarus.2005.08.022

Treiman A.H., 2003. *Geologic settings of Martian gullies: Implications for their origins*. Journal of Geophysical Research E: Planets, 108 (4), GDS 12-1-12-13.

Yue Z., Hu W., Liu B., Liu Y., Sun X., Zhao Q., Di K., 2014. *Quantitative analysis of the morphology of martian gullies and insights into their formation*. Icarus, 243, 208-221. https://doi.org/10.1016/j.icarus.2014.08.028

(Ms. received 08 May 2025, accepted 08 July 2025)